

FLOW CHARACTERISTIC INVESTIGATION OF A NOVEL
POWER-AUGMENTED WATER KINETIC TURBINE FOR
ENERGY CAPTURING FROM RIVER

CHRISTOPHER CLEMENT RUSLI

FACULTY OF ENGINEERING
UNIVERSITY OF MALAYA
KUALA LUMPUR

2021

**FLOW CHARACTERISTIC INVESTIGATION OF A
NOVEL POWER-AUGMENTED WATER KINETIC
TURBINE FOR ENERGY CAPTURING FROM RIVER**

CHRISTOPHER CLEMENT RUSLI

**RESEARCH PROJECT SUBMITTED IN PARTIAL
FULFILMENT OF THE REQUIREMENTS FOR THE
DEGREE OF MASTER OF MECHANICAL
ENGINEERING**

**FACULTY OF ENGINEERING
UNIVERSITY OF MALAYA
KUALA LUMPUR**

2021

UNIVERSITY OF MALAYA
ORIGINAL LITERARY WORK DECLARATION

Name of Candidate: Christopher Clement Rusli

Matric No: S2005385/1

Name of Degree: Master of Mechanical Engineering

Title of Project Paper/Research Report/Dissertation/Thesis (“this Work”):

Flow Characteristic Investigation of A Novel Power-Augmented Water Kinetic Turbine for Energy Capturing from River

Field of Study:

Computational Fluid Dynamics

I do solemnly and sincerely declare that:

- (1) I am the sole author/writer of this Work;
- (2) This Work is original;
- (3) Any use of any work in which copyright exists was done by way of fair dealing and for permitted purposes and any excerpt or extract from, or reference to or reproduction of any copyright work has been disclosed expressly and sufficiently and the title of the Work and its authorship have been acknowledged in this Work;
- (4) I do not have any actual knowledge nor do I ought reasonably to know that the making of this work constitutes an infringement of any copyright work;
- (5) I hereby assign all and every rights in the copyright to this Work to the University of Malaya (“UM”), who henceforth shall be owner of the copyright in this Work and that any reproduction or use in any form or by any means whatsoever is prohibited without the written consent of UM having been first had and obtained;
- (6) I am fully aware that if in the course of making this Work I have infringed any copyright whether intentionally or otherwise, I may be subject to legal action or any other action as may be determined by UM.

Candidate’s Signature

Date: 20/08/2021

Subscribed and solemnly declared before,

Witness’s Signature

Date: 30/08/2021

Name:

Ir. Dr. ALEX ONG ZHI CHAO
Senior Lecturer
Department of Mechanical Engineering
Faculty of Engineering
University of Malaya
50603 Kuala Lumpur

Designation:

**FLOW CHARACTERISTIC INVESTIGATION OF A NOVEL POWER-
AUGMENTED WATER KINETIC TURBINE FOR ENERGY CAPTURING
FROM RIVER**

ABSTRACT

Fossil fuel power plants still dominate world electricity generation. 38% of the world's electricity generation is coal, and another 23% is natural gas. Fossil power plants impact a lot on pollutant emissions. Therefore, renewable energy needs to be developed to reduce this effect. Renewable energy uses an available energy source that automatically recharges naturally—the energy sources such as sun, wind, water, Earth's heat, and plants. One of the water sources available is a river, which can generate electricity in rural areas. The hydrokinetic turbine is used to capture the available energy from the river. A lot of studies show the availability to capture water energy using a kinetic turbine. However, the efficiency of the hydrokinetic turbine is relatively low. Thus, this study is carried out to observe the augmentation design for the hydrokinetic turbine. The vertical-axis turbine two-blade with NACA0021 airfoil profile will be used for this study. The augmentation observed will be a NACA0015 profile with a chord length of 2000 mm and connected with spline tools to create the augmentation profile. Both analytical and numerical methods will be used in this study. The analytical approach is used to approximate the performance of the blade used for the turbine. The numerical method will be used to observe the flow characteristic and the efficiency of the augmentation profile. Three different pitch angles for the augmentation profile—6°, 10°, and 15° are used to enhance the hydrokinetic turbine's performance. The hydrokinetic turbine has a baseline performance of 0.397 at TSR is equal to 2.58. The augmentation profile achieved a 77.33% performance improvement with a power coefficient value of 0.704 at TSR is equal to 3.0. The positioning of the turbine is also observed because it affects the performance as well. This study finds that the positioning of the turbine can slightly

improve the performance and worsen the performance too. The power coefficient reaches the highest of 0.712 when the turbine slightly moved from the initial position. In conclusion, this study proves the significant impact of the augmentation implemented in the vertical-axis hydrokinetic turbine. The improvement of power coefficient reaches as high as 79.34% compared to the bare turbine.

Keywords: Renewable energy, hydropower, hydrokinetic turbine, augmentation device, computational fluid dynamics

Universiti Malaysia

**PENYELIDIKAN KARAKTERISTIK ALIRAN TURBIN KINETIK AIR
DENGAN ALAT PEMBESARAN DIUNTUK MEMERANGKAP TENAGA
DARI SUNGAI**

ABSTRAK

Loji janakuasa fosil masih menguasai kuasa penjanaan elektrik sedunia. 38% daripada penjanaan elektrik dunia adalah arang batu, dan 23% lagi adalah gas asli. Loji janakuasa fosil banyak mempengaruhi pelepasan bahan pencemar. Oleh itu, tenaga boleh diperbaharui perlu dikembangkan untuk mengurangkan kesan ini. Tenaga boleh diperbaharui menggunakan sumber tenaga sedia ada di mana ianya secara automatik diganti dengan cara yang semula jadi—sumber tenaga seperti matahari, angin, air, panas bumi, dan tumbuhan. Salah satu sumber air yang ada ialah sungai, yang dapat menjana elektrik di kawasan luar bandar. Turbin hidrokinetik digunakan untuk memerangkap tenaga yang ada dari sungai. Banyak kajian menunjukkan ketersediaan untuk memerangkap tenaga air menggunakan turbin kinetik. Walau bagaimanapun, kecekapan turbin hidrokinetik agak rendah. Oleh itu, kajian ini dilakukan untuk melihat reka bentuk pembesaran bagi turbin hidrokinetik. Dua bilah turbin paksi menegak dengan profil keratan udara NACA0021 akan digunakan dalam kajian ini. Augmentasi yang diperhatikan adalah profil NACA0015 dengan panjang kord 2000 mm dan dihubungkan dengan alat spline untuk membuat profil pembesaran. Kedua-dua kaedah analisis dan numerik akan digunakan dalam kajian ini. Pendekatan secara analitik digunakan untuk menganggarkan prestasi bilah yang digunakan oleh turbin. Kaedah berangka akan digunakan untuk memerhatikan ciri aliran dan kecekapan profil pembesaran. Tiga sudut nada profil pembesaran yang berbeza iaitu— 6 °, 10 °, dan 15 ° digunakan bagi meningkatkan prestasi turbin hidrokinetik. Turbin hidrokinetik mempunyai prestasi awal iaitu 0.397 pada TSR bernilai 2.58. Profil pembesaran mencapai peningkatan prestasi sebanyak 77.33% dengan nilai pekali daya 0.704 pada TSR bernilai 3.0. Kedudukan

turbin juga diperhatikan kerana turut mempengaruhi prestasi juga. Kajian ini mendapati bahwa kedudukan turbin boleh memberi sedikit pengaruh kepada peningkatan prestasi turbin namun begitu ia sekaligus mampu memburukkan prestasi. Pekali daya mencapai data yang tertinggi iaitu 0.712 apabila turbin bergerak sedikit dari kedudukan awal. Kesimpulannya, kajian ini membuktikan kesan ketara dari augmentasi yang dilaksanakan dalam turbin hidrokinetik paksi menegak. Peningkatan pekali kuasa mencapai setinggi 79.34% jika nak dibandingkan dengan turbin tanpa profil pembesaran.

Kata kunci: energi terbarukan, tenaga air, turbin air, alat pembesaran, dinamik bendalir pengiraan.

Universiti Malaya

ACKNOWLEDGEMENTS

I am very grateful for the chance to express my gratitude to my research project supervisor, Associate Prof. Dr. Chong Wen Tong, for the opportunity to research with his guidance. My knowledge is improved by working together with him. His creativity and attitude also make me enjoy the process of doing this research project.

Furthermore, I want to thank Dr. Kong Keen Kuan, who guided me through my research project. He taught me a lot during the progression of doing this research project. I am also very grateful for my family, who keeps supporting me during my study. They give a lot of love and mental support always to keep my motivation high.

Last but not least, I am very thankful for my friends in Indonesia that always keep in touch with me and listen to my hardship while doing this research. I am also grateful to be able to meet fantastic friends in Malaysia during my study. A lot of difficulties we pass through the study together. I am genuinely thankful for everyone who already is a support for me during this study.

TABLE OF CONTENTS

Abstract	iii
Abstrak	v
Acknowledgements	vii
Table of Contents	viii
List of Figures	xi
List of Tables.....	xiv
List of Symbols And Abbreviations.....	xv
List of Appendices	xviii
CHAPTER 1: INTRODUCTION.....	1
1.1 Introduction.....	1
1.2 Problem Statement.....	6
1.3 Research Objective	6
1.4 Scope of Research	7
1.5 Thesis Organization	7
CHAPTER 2: LITERATURE REVIEW	8
2.1 Introduction.....	8
2.2 Energy	8
2.3 Hydropower Generation.....	9
2.4 Reynolds Number.....	10

2.5	Boundary Layer	10
2.6	Concept of Hydrokinetic Turbine	11
2.6.1	Horizontal Axis Hydrokinetic Turbine	12
2.6.2	Vertical Axis Hydrokinetic Turbine.....	13
2.7	Augmentation of Hydrokinetic Turbine	14
2.8	Tip Speed Ratio & Solidity.....	18
2.9	Computational Fluid Dynamics (CFD)	18
CHAPTER 3: METHODOLOGY.....		20
3.1	General Description	20
3.2	Analytical Method.....	22
3.3	Numerical Method	25
CHAPTER 4: RESULT AND DISCUSSION.....		30
4.1	Analytical Result.....	30
4.2	Dependency Result.....	32
4.3.	Validation Result.....	35
4.4.1.	Flat Plate Augmentation Profile	37
4.4.2.	Airfoil Augmentation Profile	39
4.4	Discussion.....	48
CHAPTER 5: CONCLUSION AND FUTURE WORK		51
5.1	Conclusion	51

5.2 Future Work	52
REFERENCES	53
APPENDIX A.....	57
APPENDIX B.....	85
APPENDIX C	93

Universiti Malaya

LIST OF FIGURES

Figure 1.1: Turbine application graphic adapted from (Timilsina et al., 2018)	2
Figure 1.2: Visualization of augmentation in a river for hydrokinetic turbine	3
Figure 2.1: Boundary layer behavior	11
Figure 2.2: General classification of hydrokinetic turbines (Khan et al., 2009)	12
Figure 2.3: Horizontal axis hydrokinetic turbines (Khan et al., 2009)	13
Figure 2.4: Vertical axis hydrokinetic turbines (Khan et al., 2009)	14
Figure 2. 5: General classification of augmentaitons (Khan et al., 2009)	15
Figure 2. 6: Deflector configuration of Mosbahi et al. research	15
Figure 2. 7: Diffuser configuration of Elbatran et al. research	16
Figure 2. 8: (a) Daniele’s & Cairo’s configuration, (b) Rezel et al. research	17
Figure 2. 9: Three different configurations of Barbarić & Guzović research	17
Figure 3.1: Methodology flow chart of this study	20
Figure 3.2: Visualization region of the turbine	23
Figure 3.3: Numerical method flow chart	25
Figure 3.4: Visualization of the CAD used	26
Figure 3.5: Visualization of the boundary condition	28
Figure 4.1: C_L and C_D graphic on different AOA	31
Figure 4.2: Analytical result of torque coefficient	32

Figure 4.3: Torque value on a different grid spacing for the validation study	33
Figure 4.4: Visualization of mesh used for the validation study.....	34
Figure 4.5: Timestep dependency result	35
Figure 4.6: Comparison of torque coefficient for validation.....	36
Figure 4.7: Power curve of the NACA0021 blade used in this study	37
Figure 4.8: Three different flat plate augmentation profiles	38
Figure 4.9: Velocity contour of steady-state simulation on flat plate augmentation	38
Figure 4.10: Flat plate power coefficient for one revolution at TSR is equal to 2.58.....	39
Figure 4.11: Torque value on a different grid spacing for augmentation study.....	40
Figure 4.12: Three different geometry of an airfoil augmentation	41
Figure 4.13: Velocity contour on the airfoil augmentation profile.....	41
Figure 4.14: Velocity value on Y-axis location of different augmentation profiles.....	42
Figure 4.15: Power coefficient of different airfoil augmentation profiles at TSR is equal to 2.58.....	43
Figure 4.16: Torque value comparison between different airfoil augmentation profiles	44
Figure 4.17: Velocity in the stationary frame comparison of 6° and 10° airfoil augmentation profiles	45
Figure 4.18: Power curve comparison of the airfoil augmentation and bare turbine	46
Figure 4.19: Visualization of the dimensionless parameter	47

Figure 4.20: Power coefficient of 6° airfoil augmentation in a different position48

Figure 4.21: Duct geometry used in Malipeddi study (Malipeddi & Chatterjee, 2012)49

Figure 4.22: External shape design in Malippedi study (Malipeddi & Chatterjee, 2012)49

Universiti Malaya

LIST OF TABLES

Table 3.1: Validation geometry dimensions.....	27
Table 3.2: Numerical settings for this study	29
Table 4.1: Angle of Attack value.....	30
Table 4.2: Mesh dependency result using Grid Convergence Index (GCI)	
analysis for the validation study	33
Table 4.3: Mesh dependency result using Grid Convergence Index (GCI)	
analysis for the augmentation study	40

Universiti Malaysia

LIST OF SYMBOLS AND ABBREVIATIONS

Symbol	Definition
α	: Angle of attack
β	: Pitch angle
λ	: Tip speed ratio
ρ	: Density
σ	: Solidity
τ	: Torque
ω	: Rotational speed
Γ_{ω}	: Effective diffusion of turbulent kinetic energy k
Γ_k	: Effective diffusion of turbulent kinetic energy ω
ΔX	: Distance from augmentation inlet to turbine's center
A	: Area of the turbine
AOA	: Angle of attack
B	: Number of blades
c	: Chord length
CO	: Carbon monoxide
CO ₂	: Carbon dioxide
C _D	: Drag coefficient
C _L	: Lift Coefficient
C _P	: Coefficient of power
C _T	: Coefficient of torque
CAD	: Computer-aided design

Symbol	Definition
CFD	: Computational fluid dynamics
D	: Turbine's diameter
D_ω	: Cross-diffusion term
DOF	: Degree of freedom
F_D	: Drag force
F_L	: Lift Force
G_k	: Generation of turbulent kinetic energy k
G_ω	: Generation of turbulent kinetic energy ω
GCI	: Grid convergence index
h	: Actual head
H	: Turbine's height
L	: Characteristic length
NO	: Nitrogen oxide
P	: Pressure
$P_{available}$: Available power from the source
P_{out}	: Power generated from the turbine
R	: Turbine's radius
Re	: Reynold's number
SO	: Sulfur oxide
S_k	: User-defined sourced term of k
S_ω	: User-defined sourced term of ω
SST	: Shear stress transport
TSR	: Tip speed ratio

Symbol	Definition
u	: Fluid velocity
ν	: Kinematic viscosity
V_∞	: Freestream velocity
W	: Relative velocity
Y_k	: Dissipation of turbulent kinetic energy k
Y_ω	: Dissipation of turbulent kinetic energy ω

Universiti Malaya

LIST OF APPENDICES

APPENDIX A: Timestep dependency test raw data.....	57
APPENDIX B: Bare turbine power curve raw data.....	85
APPENDIX C: Airfoil augmentation power curve raw data.....	93

Universiti Malaya

Universiti Malaya

CHAPTER 1: INTRODUCTION

1.1 Introduction

According to the International Energy Agency (IEA) report, fossil fuel power plants dominate world electricity generation. 38% of the world's electricity generation is coal, and another 23% is natural gas (International Energy Agency, 2021). Thus, pollutant emissions from fossil fuel power plants such as NO_x , SO_x , CO_2 , and CO are still high and harm humans and the Earth (Fouladi Fard et al., 2016). In 2018, about 93% of U.S. anthropogenic CO_2 emissions were caused by fossil fuel powerplant combustion (Administration, 2020). Therefore, it is crucial to develop renewable energy to reduce the emissions and any adverse effect of fossil fuel powerplant.

Renewable energy utilizes an available energy source that automatically recharges naturally—the energy sources such as sun, wind, water, Earth's heat, and plants are called renewable energy. The technology used to utilize these sources to produce usable energy such as electricity, heat, and mechanical power (Holt & Pengelly, 2008). Thus, it is crucial to utilize renewable energy to reduce fossil fuel power, which caused many emissions. Hydropower potential is still abundant on Earth, which around 82% of the available hydropower is still not utilized in Asia-Pacific (Bank et al., 2019). Thus, development in hydropower technology is needed to use the available hydropower potential in the world. There are many types of water turbine technology that can be used to converge energy to electricity. A different kind of water turbine is suitable for various water conditions. A lot of traditional water turbine is ideal for having a large head or a large water flowrate. However, many potentials have a small available head and low flowrate conditions located in rural areas. Thus, the hydropower built in these conditions is called pico-hydro, which generates power only up to 5 kW. Pico-hydro has some advantages, such as ease to manufacture, low investments, and low operating costs than other sustainable energy

technology (Ho-Yan, 2012). It is crucial to develop pico-hydro technology to utilize the available energy to help rural areas.

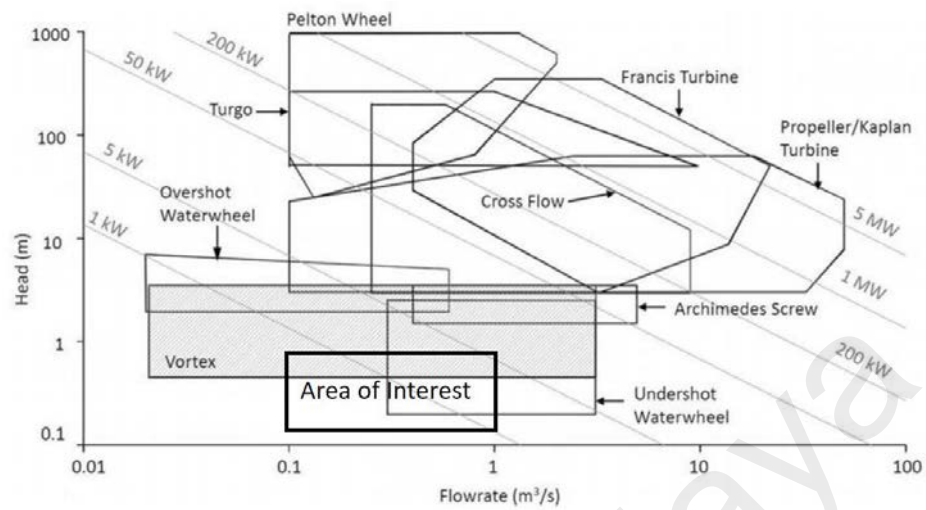


Figure 1.1: Turbine application graphic adapted from (Timilsina et al., 2018)

Darrius water turbine is one of the hydrokinetic turbines used effectively for this geographical condition without building any extra structure in the river. Darrius water turbines can also work without harming any biological creature in the environment (Maître et al., 2013). The Darrius water turbine takes advantage only of the kinetic energy available in the water, which is compatible with river run-off conditions. However, this turbine has significantly low efficiency, but many modifications can be done to improve the efficiency of the Darrius water turbine. One modifier is building an augmentation around the water turbine to improve the power coefficient. The augmentation will cause an enhancement of velocity before hitting the turbine's blade. It has also caused a pressure difference before and after the water turbine, creating a suction effect from high to low pressure. Fig. 1.2 will show the visualization of the augmentation place in the river. Therefore, developing a better design and modification of the Darrius water turbine can achieve higher and optimum efficiency.

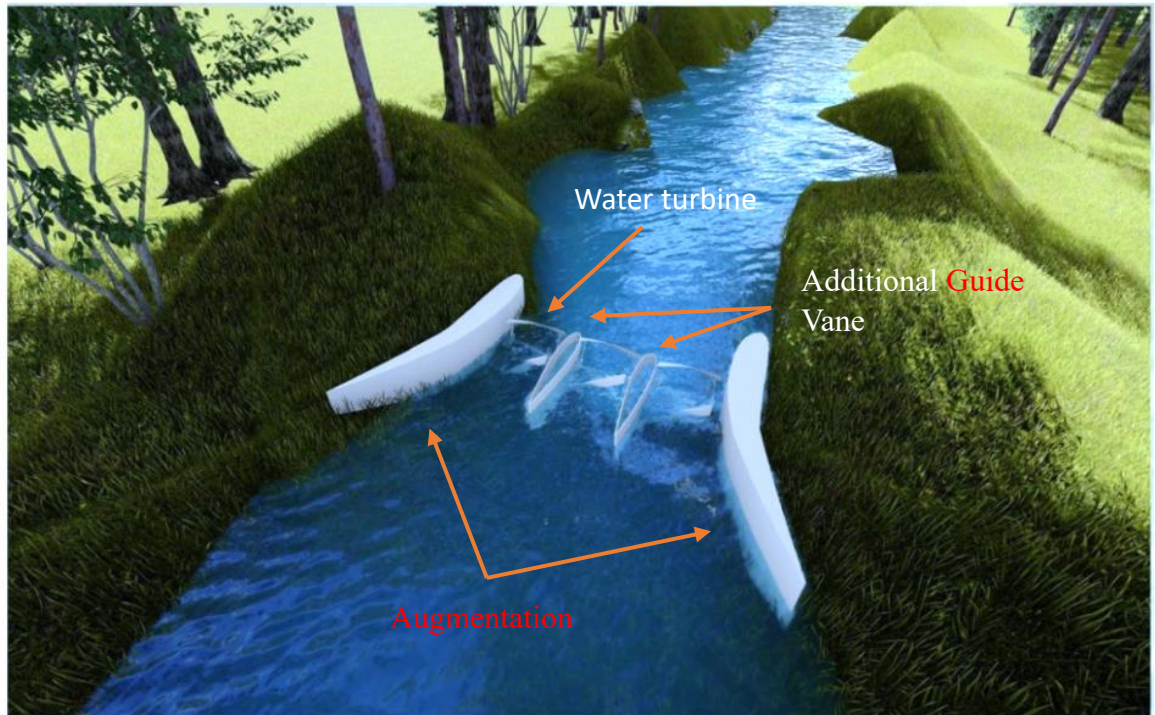


Figure 1.2: Visualization of augmentation in a river for hydrokinetic turbine

A lot of the previous study has been done regarding the Darrieus water turbine. Mc Adam et al. had done experimental work around the Darrieus water turbine with a NACA0018 blade profile (McAdam et al., 2013). In their study, many different configuration experimental setups were carried out and observed which configuration achieved the best performance. Their study proves that placing the Darrieus water turbine cross-flow or vertically only affected a reduction of peak power generated of 0.98, which is not significant. Their research also mentions that higher power output can be achieved with a higher blockage ratio. These findings are reinforced by Patel et al. (Patel et al., 2019). However, in their research, it can be seen clearly that the blockage placement and dimensions affect the power output significantly. Their study using a specific dimensionless number for the width and the location of the blocking plate. A $0.28D$ width of the blocking plate was used to achieve the highest power coefficient in their research. The block placement is at $0.48D$ spanwise from the rotor center to the block center and $0.57D$ streamwise. Tunio et al. did a duct augmented system for the Darrieus turbine

(Tunio et al., 2020). In their study, a comparison between ducted and non-ducted channels was conducted. The ducted system's power output is higher than in non-ducted because the flow velocity increases when the area becomes smaller. The ducted system also changes the velocity vector hitting the blade profile of the turbine. Their study also observed that the stress became twice higher compared to the non-ducted system. They conclude that the power production increases 112% in the ducted system compared with non-ducted.

These findings align with the previous research by Malipeddi et al. (Malipeddi & Chatterjee, 2012). In their study, the ducted shape indeed shows an increase in the power coefficient. Moreover, the external geometry of the duct also affects the turbine's coefficient power. The change in coefficient power happens because the ducting's external geometry affects the turbine's flow, which affects the pressure. If the pressure around the turbine is lower because of the duct's external geometry, there will be a suction effect that caused the increase of the power coefficient. There are also other methods to improve the power generated from the water turbine. Hybridization of the Darrieus turbine with Savonius is the most popular thing, and a lot of research investigates the hybrid model of these turbines. Fertahi et al. research three different hybrid models (ed-Dîn Fertahi et al., 2018). The first model has synchronous coupling, which means the direction of the rotation is identical. The second model has asynchronous coupling, but the direction of the rotation is the opposite. The last model has asynchronous coupling, and the direction of the rotation is identical. This study concludes that the best configuration of the hybridization is asynchronous coupling with identical rotation direction compared to the other two. In 2020, other researchers, Saini's brother, proved that hybridization achieves better performances than the single Darrieus turbine (Saini & Saini, 2020). Their study compared the performances of hybrid turbine and single

Darrieus turbine both numerically and experimental. The torque coefficient fluctuates less for hybrid rotor which reduce the stress of the turbine body.

Numerical method improvements have also been made by many different researchers on the Darrieus turbine case study. Fleisinger et al. research compare their advanced flow-driven simulation based on transient sliding mesh procedure and six degrees of freedom (6-DOF) simulation (Fleisinger et al., 2014). Their validation study achieved that the 6-DOF is more accurate to the experimental data than their advanced flow-driven simulation. However, the computational speed for the 6-DOF simulation is longer than the developed flow-driven simulation by Fleisinger et al., which is entirely accurate in achieving the numerical result. In 2019, Benchikh et al. research a numerical approach of using the multiphase Volume of Fluid (VoF) method on other experimental cases that have been published (Benchikh Le Hocine et al., 2019). In their study, the turbulence model used is $k - \omega SST$, and 2-dimension simulation. Their study present that there will be so much overprediction by 42.4% and 26.6% for power and torque coefficients, mainly due to the disregard of free surface in single-phase simulation. Another research named Maître et al. found that the wall grid refinement significantly affects the numerical result (Maître et al., 2013). Their study proves that increasing y^+ values will be decreasing the power coefficient rapidly. The coarse grid at the wall will cause an unrealistic drag caused by a bubble developing when the blade is rotating.

A lot of performance enhancement has been developed from the previous study. The enhancement comes from the ducted channel, blockage downstream, hybridization turbine, and diffuser. However, there is still no mutual agreement between the geometry profile for the diffuser. In previous Roa et al. research, the aerofoil profile diffuser can improve 2.5 until 3.5 times (Roa et al., 2010). However, in the recent diffuser study by Barbarić & Guzović, the best geometry profile was achieved not by aerofoil type but by another geometry profile called DFB configuration (Barbarić & Guzović, 2020). Because

of that, a power enhancement will be carried out by comparing different augmentation geometries and adding guide vane or blockage the downstream before the augmentation.

1.2 Problem Statement

Renewable energy development needs to be improved to achieve sustainable development goals in affordable and clean energy. This type of water turbine can help attain affordable clean energy for rural areas and other places suitable for run-off river turbines. However, the Darrieus water turbine has a lower performance coefficient compared to other water turbines. Because of that, a performance enhancement needs to be carried out to optimize the output of this turbine. The performance can be increased by changing the blade aerofoil type. However, this method is complicated in manufacturing and more expensive. It is more feasible to make a diffuser to enhance the performance of the water turbine. This study would like to research the optimum augmentation geometry profile and further improve the performance of the water turbine using the computational fluid dynamics (CFD) numerical method.

1.3 Research Objective

This research wants to develop a suitable diffuser geometry for improving the Darrieus water turbine performance. Some objectives needed to be achieved to complete the investigation, such as:

1. To develop a suitable augmentation that works well with the vertical axis hydrokinetic turbine.
2. To investigate the hydrodynamics behavior and flow characteristics on the vertical axis hydrokinetic turbine.

1.4 Scope of Research

This research aims to find a suitable diffuser for improving the efficiency of the Darrieus water turbine, using computer-aided design (CAD) to design and later imported to computational fluid dynamics (CFD) software to observe and analyze the hydrodynamics behavior and flow characteristic. The performance of the water turbine will be investigated by the CFD software as well. Because of that, the numerical method validation for this research will be done by comparing the numerical method of this study with the previous research available.

1.5 Thesis Organization

Chapter 1: In this chapter, the energy condition of the world is discussed and the importance of improving available renewable energy in the world. The problem statement and objective of the research are mentioned in this chapter as well.

Chapter 2: This chapter will discuss the fundamental energy conversion of water turbines and the literature review about hydrokinetic turbines.

Chapter 3: In this chapter, the method used for this research will be explained thoroughly. The methods used for this research will be the analytical method to measure the theoretical performance and the numerical method to measure the performance more accurately.

Chapter 4: In this chapter, the discussion of the founding through the numerical method will be explained here and compared to the literature study or previous findings.

Chapter 5: In this chapter, the conclusions of this research and the future work suggestion will be written in this section.

CHAPTER 2: LITERATURE REVIEW

2.1 Introduction

The importance of understanding energy conversion is crucial for hydropower generation. In hydropower generation, the energy available from the water itself consists of kinetics or potential. Moreover, the water flow contains many fluid mechanics understanding, such as Reynold's number, boundary layer, and concept of a hydrokinetic turbine. The literature review regarding hydropower generation and the Darrieus turbine will be reviewed.

2.2 Energy

Energy is something that cannot be created, and the overall energy is conserved. The conservation of energy is a similar concept to the conservation of mass. However, energy can be converted into different energy forms (Mehling, 2017). In hydropower generation, the available kinetic energy from the water is transformed into mechanical energy to electricity with the help of the water turbine.

Fluids mechanics have three different energy forms: pressure, kinetics or dynamics pressure, and potential. These three energy forms can be expressed in an equation which is called Bernoulli's equation. This equation is the most commonly used in the calculation of fluid energy. However, this equation can only be used at steady-state flow. Bernoulli's equation also ignores losses resulting from fluid friction. Bernoulli's equation can be stated by Eq. (2.1):

$$\begin{aligned} \text{Total Initial Energy} &= \text{Total Final Energy} \\ P_1 + \frac{1}{2}\rho v_1^2 + \rho g h_1 &= P_2 + \frac{1}{2}\rho v_2^2 + \rho g h_2 \end{aligned} \quad (2.1)$$

P is pressure, ρ is density, v is flow velocity, g is gravity, and h is the height of the flow position.

A flow condition with a flow rate and a velocity has a potential power that can be generated. This power can be written by Eq (2.2):

$$P_{available} = \frac{1}{2} \rho A V_{\infty}^3 \quad (2.2)$$

V_{∞} is a free flow velocity, and A is an area of the turbine that the water hits. Eq. (2.2) can be used for calculates the hydraulic efficiency or coefficient of power of the water turbine. The power output and coefficient power can be calculated by Eq (2.3 & 2.4):

$$P_{out} = \tau \omega \quad (2.3)$$

$$C_p = \frac{P_{out}}{P_{available}} \quad (2.4)$$

τ is a torque produced by the turbine, ω is angular velocity.

2.3 Hydropower Generation

In hydropower generation, the essential factor is the availability of the site condition. Because of that, the water turbine is categorized into two basic types, impulse, and reaction (Munson et al., 1994). The available head (pressure, velocity, and potential head) is converted into an enormous speed using the nozzle in the impulse turbine. However, in the reaction turbine, part of the pressure energy is converted into kinetic energy. The kinetic energy captured by the turbine blades causes a changed in pressure after the flow leaves the turbine.

A hydrokinetic turbine is a reaction-type turbine that only utilizes the available kinetic energy available in the water. This type of turbine is usually used for river, ocean, and current tidal conditions. The hydrokinetic turbine does not need additional civil construction caused it can use pre-existing structures such as bridges and canals for its support, unlike traditional water turbines that need large dams. However, there are some disadvantages of hydrokinetic turbines. The installation cost is significantly higher

compared to other renewable energy such as solar. The environmental impact is also still unsure whether it will cause harm to marine ecology.

2.4 Reynolds Number

Reynolds number is a dimensionless dimension that represents the ratio between inertial forces to viscous forces. The Reynolds number shows the effect of viscosity is significant in the fluid flow pattern. The Reynolds number is used to decide whether the flow is laminar or turbulent flow. It is categorized that Reynolds number is equal to or less than 2100 is a laminar flow, and greater than 2100 indicates turbulent flow. Laminar flow means that the fluid's viscosity is dominant than the inertial forces, making the fluid flow constant and smooth. However, the turbulent flow is dominated by inertial forces, which produce many eddies, vortices, and other flow instabilities (Carlton, 2012). Reynolds number equation can be stated by Eq (2.5):

$$Re = \frac{uL}{\nu} \quad (2.5)$$

u is a fluid velocity, L is the characteristic length or the chord length of an airfoil, ν is the kinematic viscosity of the fluid.

2.5 Boundary Layer

The boundary layer is a region that occurs because of a bounding surface where the fluid's viscosity is significant. The boundary layer size and structure can be diverse, dependent on the shape of the object. The simplest thing to represent the boundary layer is a flow over a flat plate. The difference between laminar and turbulent boundary layer behavior on the flat plate can be seen in Fig. 2.1. It can be seen that in the turbulent boundary layer, the fluid particle inertial force is causing vortices and eddies (Munson et al., 1994).

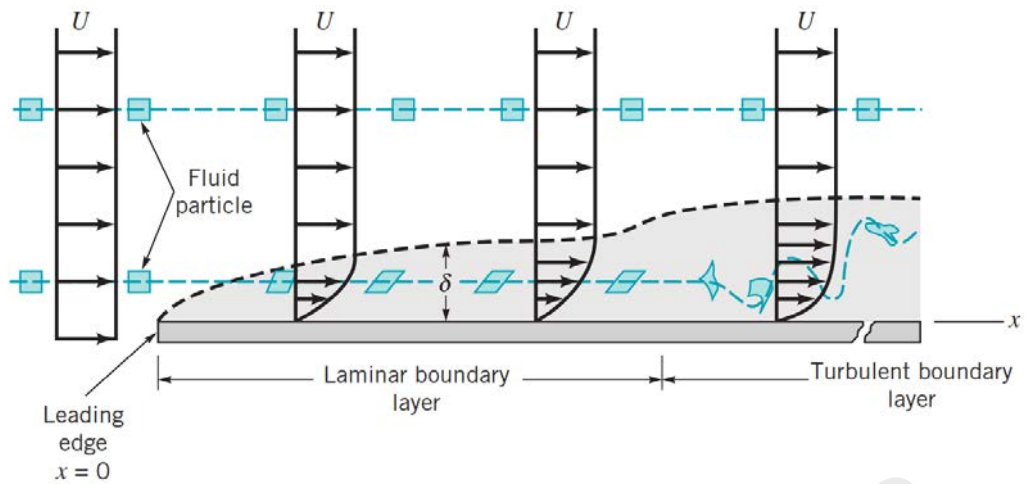


Figure 2.1: Boundary layer behavior

2.6 Concept of Hydrokinetic Turbine

The general classification of hydrokinetic turbine consists of the horizontal axis, cross-flow, and vertical axis. Horizontal axis hydrokinetic turbine is the rotor parallel to the incoming water stream. The vertical axis hydrokinetic turbine is the rotor vertical to the water surface and the incoming water stream orthogonal. The cross-flow hydrokinetic turbine rotates parallel to the water surface, but the water stream is orthogonal. All of these hydrokinetic turbines use the lift or drag type of blades to convert the energy. Fig. 2.2 shows the general classification of the hydrokinetic turbine. Many concepts are developed and adopted from wind power generation.

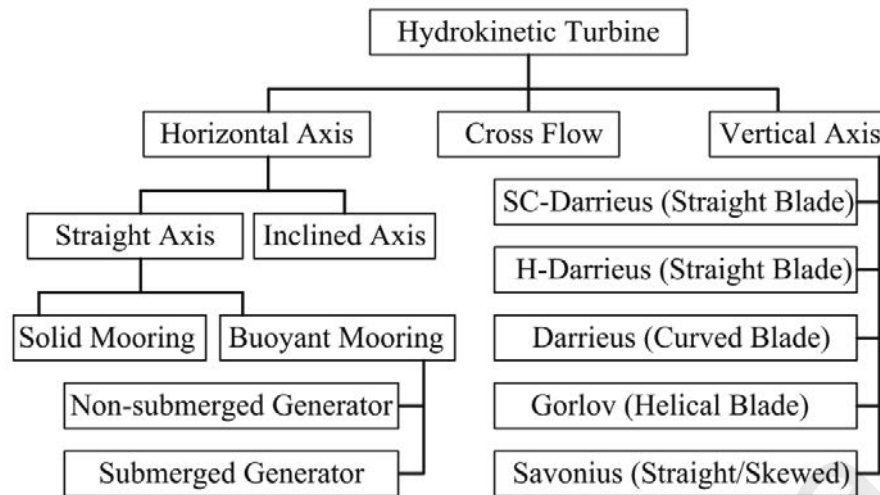


Figure 2.2: General classification of hydrokinetic turbines (Khan et al., 2009)

2.6.1 Horizontal Axis Hydrokinetic Turbine

The horizontal axis hydrokinetic turbine works very similarly to the conventional wind turbine. The important factor from this type of turbine is the blade profile and the swept area. Fig. 2.3 shows the configuration of the existing horizontal axis hydrokinetic turbine. It can be seen that the difference is only the structural mounting of the turbine. The energy conversion is the same as conventional wind power generation. The water or tidal current hits and rotates the rotor which the rotor axis is parallel to the water stream. The horizontal axis is easy to self-start but has a faster operating tip speed ratio (TSR) (Khan et al., 2009).

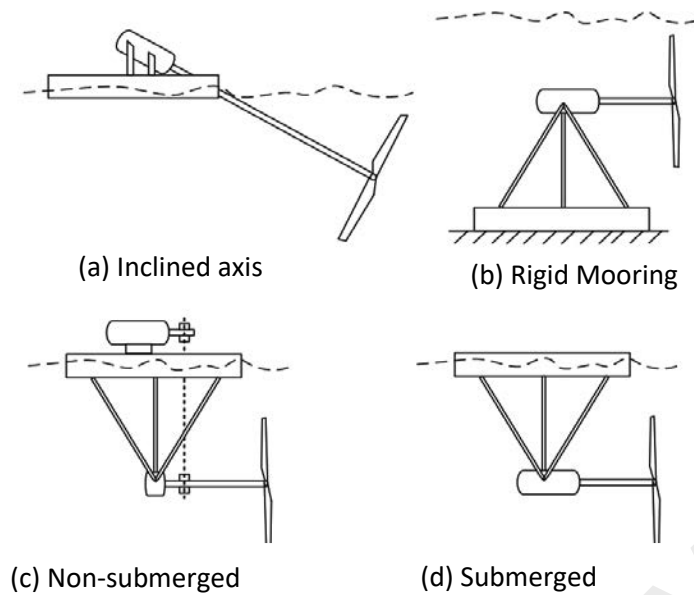


Figure 2.3: Horizontal axis hydrokinetic turbines (Khan et al., 2009)

2.6.2 Vertical Axis Hydrokinetic Turbine

The vertical axis hydrokinetic turbine consists of a lot of designs. Fig. 2.4 shows the available vertical axis models that have been developed. There are a lift type (Darrieus) and drag type (Savonius). The vertical axis turbine has a rectangular cross-section area characteristic, which provides better energy availability than the horizontal axis. However, the vertical axis's disadvantage is that it needs a higher velocity to self-start (Niebuhr et al., 2019). Because of the pulsating torque, the cross-section, which should provide better energy availability, cannot be converted efficiently by a vertical axis hydrokinetic turbine. The torque of the vertical axis is not as smooth compared to the horizontal axis, which causes the generation is not as smooth as the horizontal axis. The cross-flow axis hydrokinetic turbine is similar to the vertical axis. Only the rotor rotates in-plane axis with the water surface (Laws & Epps, 2016). Both vertical and cross-flow do not need yawing mechanisms because the water stream in the river is coming from one direction only (Bachant & Wosnik, 2015).

A development for improving the power coefficient was already done previously by analyzing the airfoil profile. Some researchers try to improve more by hybridizing both the Savonius and Darrieus turbine to achieve more power. This hybridization is working since a lot of flow in the Darrieus turbine is not utilized maximally, so the Savonius turbine helps capture the remaining kinetic energy. The hybridization can make the torque less fluctuate and reduce the rotor body's stress (Saini & Saini, 2020).

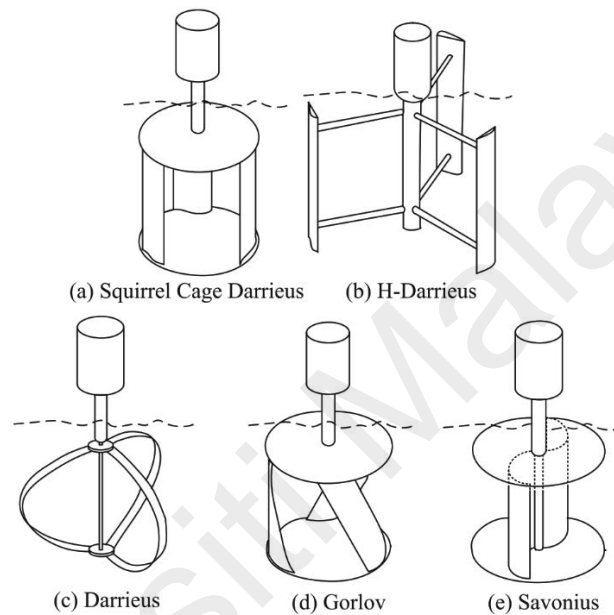


Figure 2.4: Vertical axis hydrokinetic turbines (Khan et al., 2009)

2.7 Augmentation of Hydrokinetic Turbine

Hydrokinetic turbine relatively has a small hydraulic efficiency. Because of that, an augmentation is developed to enhance the efficiency of the turbine further. In general, the type of augmentation can be seen in Fig. 2.5 (Khan et al., 2009). The diffuser type is more commonly used, and the rectilinear geometry is used in horizontal-axis turbine configuration. The curvilinear diffuser type is frequently used to enhance the vertical-axis turbine configuration.

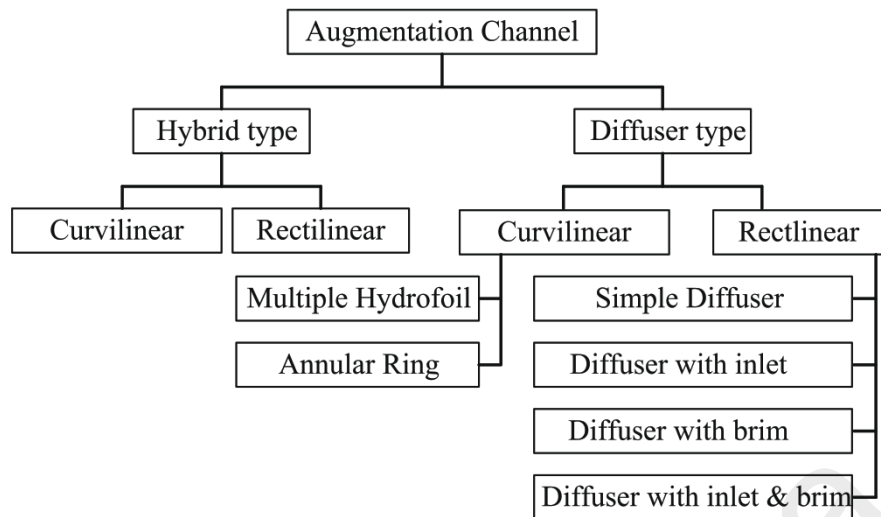


Figure 2. 5: General classification of augmentaitons (Khan et al., 2009)

Mosbahi et al. researched using a deflector rather than a diffuser to enhance the hydraulic efficiency (Mosbahi et al., 2019). Their study found that the efficiency can increase by using a simple airfoil profile to deflect the flow into the turbine. The helical Savonius blade is used for their research. It affects efficiency because the flow will hit the helical blades optimally when deflected at a correct angle. Hence, the momentum absorbed increases the hydraulic efficiency of the turbine. The power coefficient of their study improved a little bit compared to the bare turbine. The configuration of their research can be seen in Fig 2.6.

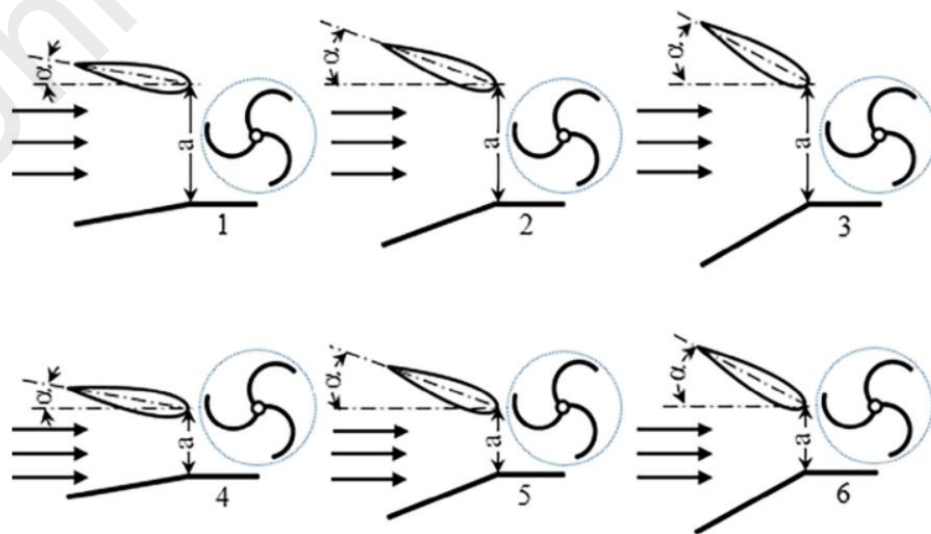


Figure 2. 6: Deflector configuration of Mosbahi et al. research

Elbatran et al. researched a diffuser using a horizontal axis marine current turbine (Elbatran et al., 2016). Their experiment proved that using an annular ring diffuser and the hydraulic efficiency can increase by 1.7 times for their study. They use inlet and outlet diffusers to enhance the performance of the turbine. The design concept of their study can be seen in Fig. 2.7.

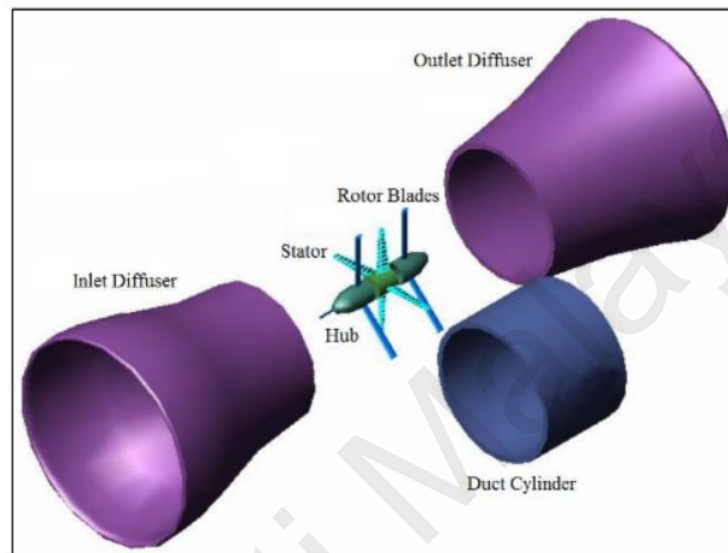


Figure 2. 7: Diffuser configuration of Elbatran et al. research

Daniele & Coiro research that the diffuser with an optimized airfoil design can reach the coefficient of power exceeding one and further (Daniele & Coiro, 2013). Rezel et al. also found a similar finding that using airfoil geometry on the diffuser can reaching the coefficient of power around one (Rezek et al., 2021). Both of these works use an actuator disk rather than an actual turbine. Without no hydraulic efficiency from the turbine, the diffuser's performance is high and can exceed a power coefficient of more than 1. The diffuser geometry is generated using their code generator to find the optimal diffuser study for their study. The configuration of their research can be seen in Fig. 2.8.

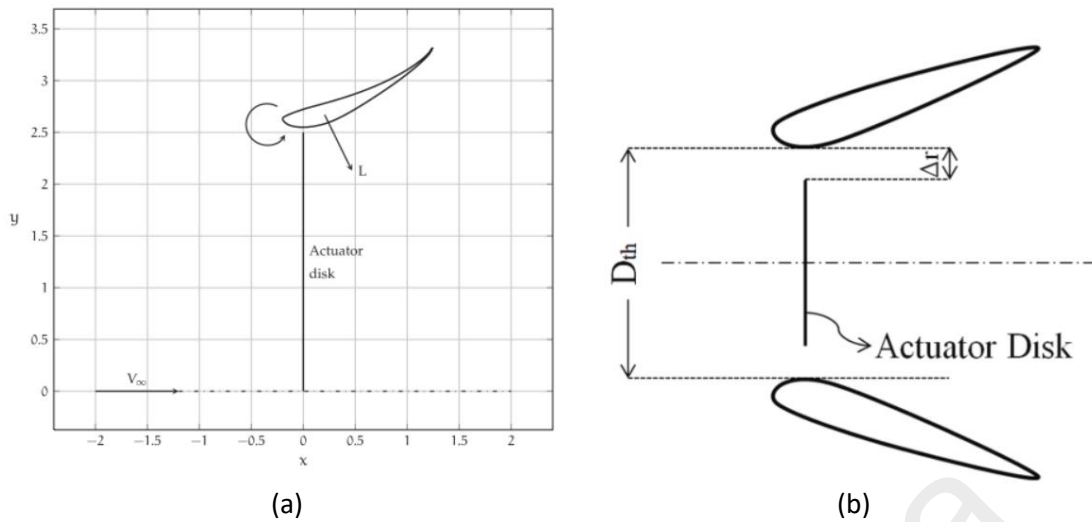


Figure 2. 8: (a) Daniele's & Cairo's configuration, (b) Rezel et al. research

However, Barbarić & Guzović conclusions are different compared to them (Barbarić & Guzović, 2020). They researched with three different diffuser configurations, as can be seen in Fig. 2.9. Their study found that the diffuser with a brim is the best enhancement, improving up to 80% of the power coefficient. Compared to the airfoil profile, the power coefficient only achieves an improvement of 40%, which is really low compared to other researchers.

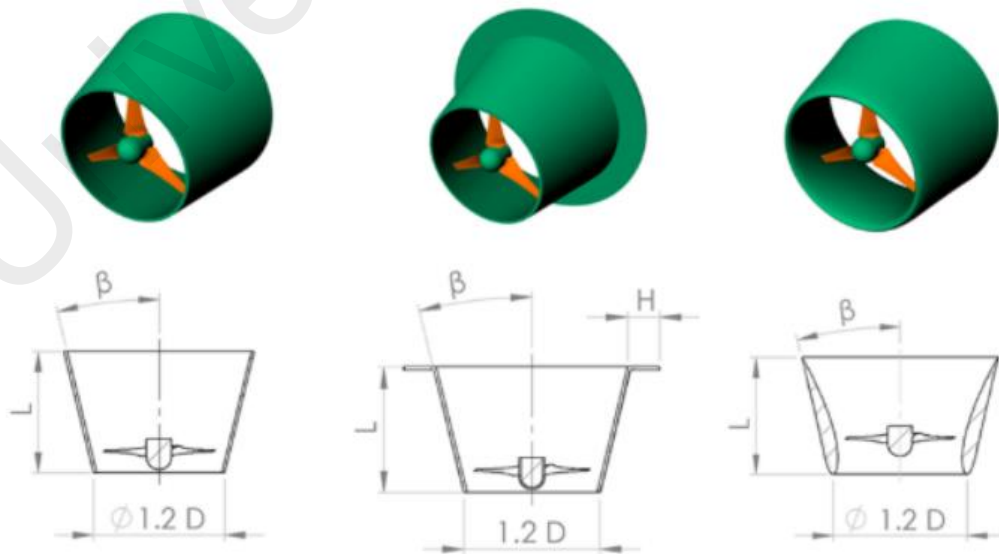


Figure 2. 9: Three different configurations of Barbarić & Guzović research

2.8 Tip Speed Ratio & Solidity

Tip Speed Ratio (TSR) is a ratio between the angular velocity on the tip of the blades to free stream velocity. If the turbine working TSR is high, the angular velocity is higher than the free stream current, causing the turbine to rotate more and have a higher centrifugal force. The higher centrifugal force can easily cause a structural failure of the blade. Posa et al. also show that the TSR affects the blades' wake region (Posa, 2020). At high TSR, the wake recovery is faster due to the instability of the shear stress generated at leeward and windward of the wake. The tip speed ratio equation can be stated as follow:

$$\lambda = \frac{\omega R}{V_{\infty}} \quad (2.6)$$

ω is the angular velocity, R is the radius of the turbine, and v is the free stream velocity.

Solidity is a ratio of total blade area to the sweeping area of the turbine. Solidity affects the flow behavior when hitting the blade turbine. Higher solidity causes the flow to have a wake behind the blades when flowing through the edges. Solidity also changes the coefficient of power curves. The working TSR of the turbine will be lower when the solidity is higher. Li et al. prove that the power curve's coefficient curve shifts when the solidity is higher (Li et al., 2016). However, the coefficient of power is slightly higher when the solidity is high. The solidity equation can be stated as follow:

$$\sigma = \frac{c B}{A} \quad (2.7)$$

B is the number of the blades, c is the chord length, and A is the turbine's swept area.

2.9 Computational Fluid Dynamics (CFD)

Computational Fluid Dynamics (CFD) is a numerical solution tool to analyze a fluid flow by mathematically modeling the physics of the fluid flow. CFD is beneficial to the

research and development phase because it can be done without prototyping and wasting money. The CFD software used is ANSYSTM Fluent®, which uses a Finite Volume Method (FVM) to solve the Navier-Stokes equation. The CFD is used to achieve power curve, power coefficient, and other parameters on each different augmentation profile in this research. All the simulations will be done using SST $k - \omega$ turbulence model. The governing equation of the turbulence model can be seen in Eq. (2.8 & 2.9):

(k)

$$\frac{\partial(\rho k)}{\partial t} + \frac{\partial(\rho k u_i)}{\partial x_i} = \frac{\partial}{\partial x_j} \left(\Gamma_k \frac{\partial k}{\partial x_j} \right) + G_k + Y_k + S_k \quad (2.8)$$

(ω)

$$\frac{\partial(\rho \omega)}{\partial t} + \frac{\partial(\rho \omega u_i)}{\partial x_i} = \frac{\partial}{\partial x_j} \left(\Gamma_\omega \frac{\partial \omega}{\partial x_j} \right) + G_\omega + Y_\omega + S_\omega + D_\omega \quad (2.9)$$

where, G_k and G_ω represent the generation of k and ω dissipation due to mean velocity gradients, Γ_k and Γ_ω represent the effective diffusivity of k and ω , Y_k and Y_ω represent the dissipation of k and ω , D_ω represents the cross-diffusion term, and S_k and S_ω are user-defined source terms (Davidson, 2015).

CHAPTER 3: METHODOLOGY

3.1 General Description

This chapter will present and discuss the flow chart of the methodology used in this study. The flow chart can be seen in Fig. 3.1, which shows the general idea of this research flows. First, the literature review is a crucial phase in the beginning. The literature review will be helpful to find a gap between previous work and this research. The literature review shows that the augmentation for vertical axis turbine is not abundantly discussed. A lot of augmentation is done for the horizontal axis turbine. Some previous research conducted about ducted turbines for the vertical axis turbine has been developed and proved to enhance the performance.

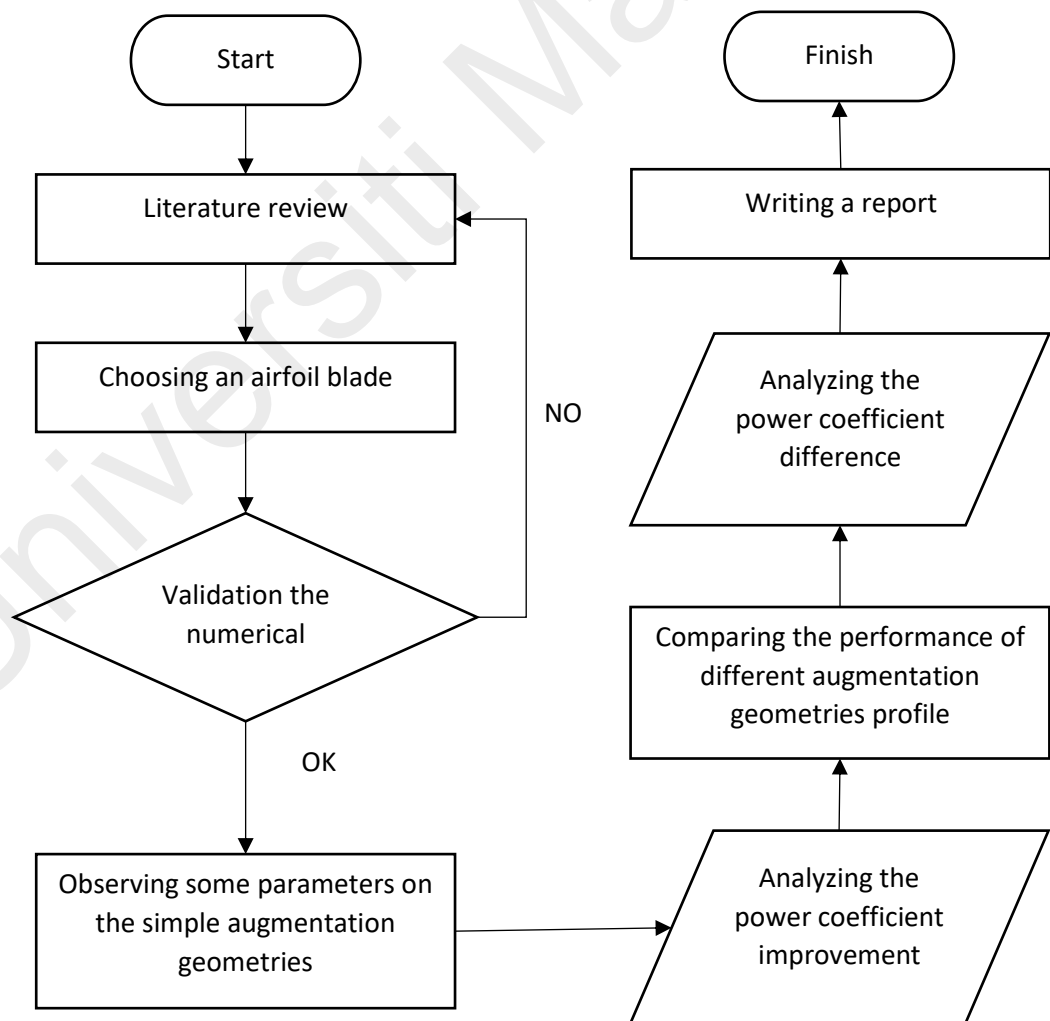


Figure 3.1: Methodology flow chart of this study

The next step is choosing the airfoil blade used for this research. In this study, a NACA0021 airfoil profile is selected for the profile. This symmetrical airfoil blade is preferred because it is easy to get and not complex to manufactured. Many data regarding vertical axis turbines using this airfoil make it easier to validate the numerical work. There are far better airfoil profiles regarding the flow condition, which can capture the kinetic energy available. However, the main idea is to observe the improvement using augmentation, so the symmetrical NACA0021 is selected compared to using complex airfoil.

After the airfoil is chosen, the validation for the numerical method is done, comparing the result with Wong et al. previous work (Wong et al., 2018). The validation is crucial to prove that the numerical method used for this research is reliable enough and accurate to use. The parameters compared to Wong et al. are coefficient of torque and coefficient of power. The validation simulation is done with TSR is equal to 2.58. The result of the validation will be discussed further in Chapter 4.

The next step is to do a steady-state simulation to observe the improvement by the augmentation device both of the flat plates and airfoil profile augmentations. After that, the exact geometry of the turbine is used to do some parametric analysis with a simple plate augmentation. The purpose of this is to prove how significantly the angle of the plate affects the power coefficient and how effectively using a simple augmentation design enhanced the power coefficient of the turbine. Later, the simple augmentation design will be compared to an airfoil augmentation geometry profile. The flow characteristic will be observed and analyzed to establish which geometry type works better for the augmentation. The power coefficient, torque coefficient, and flow behavior will be observed and discussed as well.

The positioning of the rotor in the augmentation also affects the overall power coefficient of the turbine. After the suitable augmentation geometry profile is established, the rotor placement will be observed using a dimensionless parameter. The dimensionless parameter used is a ratio of the rotor's diameter to the inlet of the augmentation length. The optimum position of the water turbine is crucial because it can affect the velocity vector hitting the blades, which will affect the power coefficient.

3.2 Analytical Method

This method calculates the approximate theoretical power curve of the symmetrical NACA0021 used for the turbine blade. Approximating the theoretical power will follow Han et al. (Han et al., 2018). In the vertical axis turbine, the angle of attack is changing as the turbine is rotating. The change is caused by the blade tip velocity and vector of the free stream velocity. The vector sum of these velocities can be calculated by Eq. (3.1):

$$W = \sqrt{V_{\infty}^2 [(\lambda - \sin^2 \theta)^2 + \cos^2 \theta]} = V_{\infty} \sqrt{1 + 2\lambda \cos \theta + \lambda^2} \quad (3.1)$$

V is the free stream velocity, λ is TSR, θ is the azimuth angle of the blade, and W is the vector sum or relative velocity.

When the turbine rotates, the angle of the blade is kept changing and causes the vector sum to change as well. The angle of attack is the angle between the vector sum and the chord length axis. Hence, the upper region of the turbine has a positive angle of attack and a negative value in the bottom region. The region of the turbine can be seen in Fig. 3.2 to visualize clearly. The angle of attack can be written as Eq. (3.2):

$$\alpha = \tan^{-1} \left(\frac{\sin \theta}{\cos \theta + \lambda} \right) - \beta \quad (3.2)$$

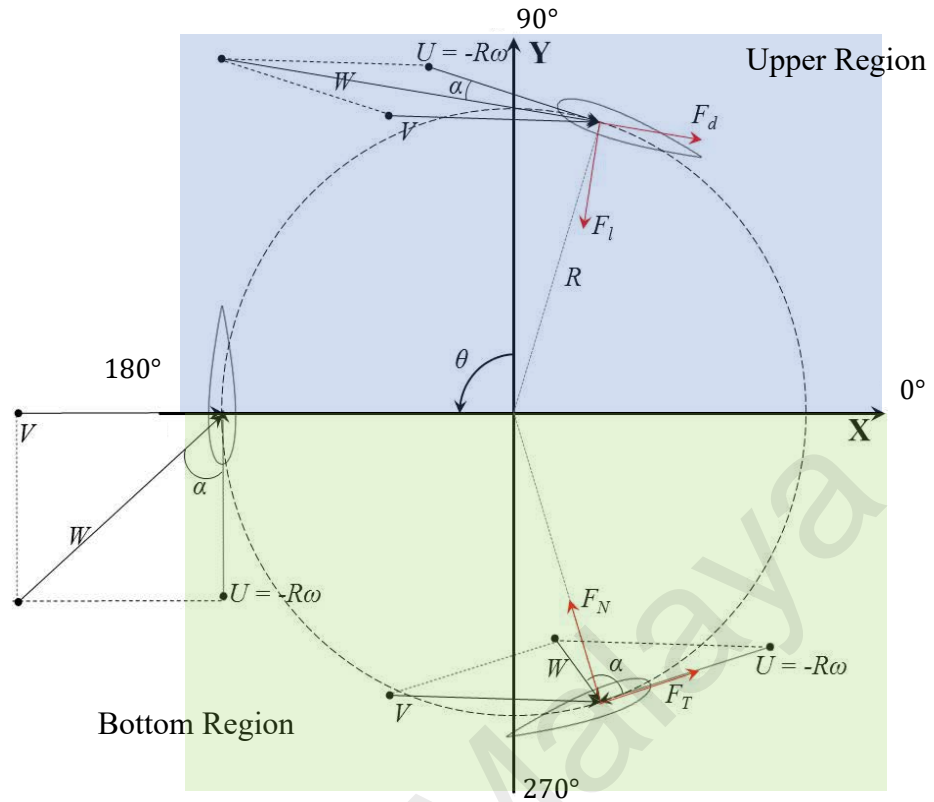


Figure 3.2: Visualization region of the turbine

After that, the lift and drag coefficient can be calculated with Eq. (3.3 & 3.4). However, the F_D and F_L values must be generated by CFD simulation or references to calculate the lift and drag coefficient.

$$C_L = \frac{F_L}{\frac{1}{2} \rho c H W^2} \quad (3.3)$$

$$C_D = \frac{F_D}{\frac{1}{2} \rho c H W^2} \quad (3.4)$$

C_L and C_D are lift and drag coefficient, F_L and F_D are lift and drag force, c is chord length, H is the blade depth, and W is relative velocity.

The lift and drag coefficient results will be used to calculate the forces that occur in the blade. There will be normal and tangential forces that happen on the airfoil blade. These forces can be calculated by calculating the normal and tangential coefficient values

using Eq. (3.5 & 3.6). Thus, the normal and tangential force values can be achieved using Eq. (3.7 & 3.8). Finally, the blade torque and power output of the blade and turbine can be calculated using Eq. (3.8 – 3.11).

$$C_{Normal} = C_L \cos \alpha + C_D \sin \alpha \quad (3.5)$$

$$C_{Tangential} = C_L \sin \alpha - C_D \cos \alpha \quad (3.6)$$

$$F_N(\theta) = \frac{1}{2} \rho c H W^2 C_N \quad (3.7)$$

$$F_D(\theta) = \frac{1}{2} \rho c H W^2 C_D \quad (3.8)$$

$$T(\theta) = \frac{1}{2} \rho c H W^2 C_T R \quad (3.9)$$

$$P(\theta) = T(\theta) \times \omega \quad (3.10)$$

$$P_{avg} = \frac{B}{2} \pi \int_0^\pi P(\theta) d\theta \quad (3.11)$$

After the torque and power had been calculated, they can be changed into dimensionless parameters called the torque coefficient (C_T) and power coefficient (C_P) by using Eq. (3.12 & 3.13). Torque coefficient is a ratio of torque generated by the turbine to the torque caused by the freestream current speed. Thus, the power coefficient is similar to the power generated to the available power from the freestream velocity.

$$C_T = \frac{T}{\frac{1}{2} \rho A R (V_\infty)^2} \quad (3.12)$$

$$C_P = \frac{P}{\frac{1}{2} \rho A R (V_\infty)^3} = \frac{T \times \omega}{\frac{1}{2} \rho A R (V_\infty)^3} = C_T \times \lambda \quad (3.13)$$

3.3 Numerical Method

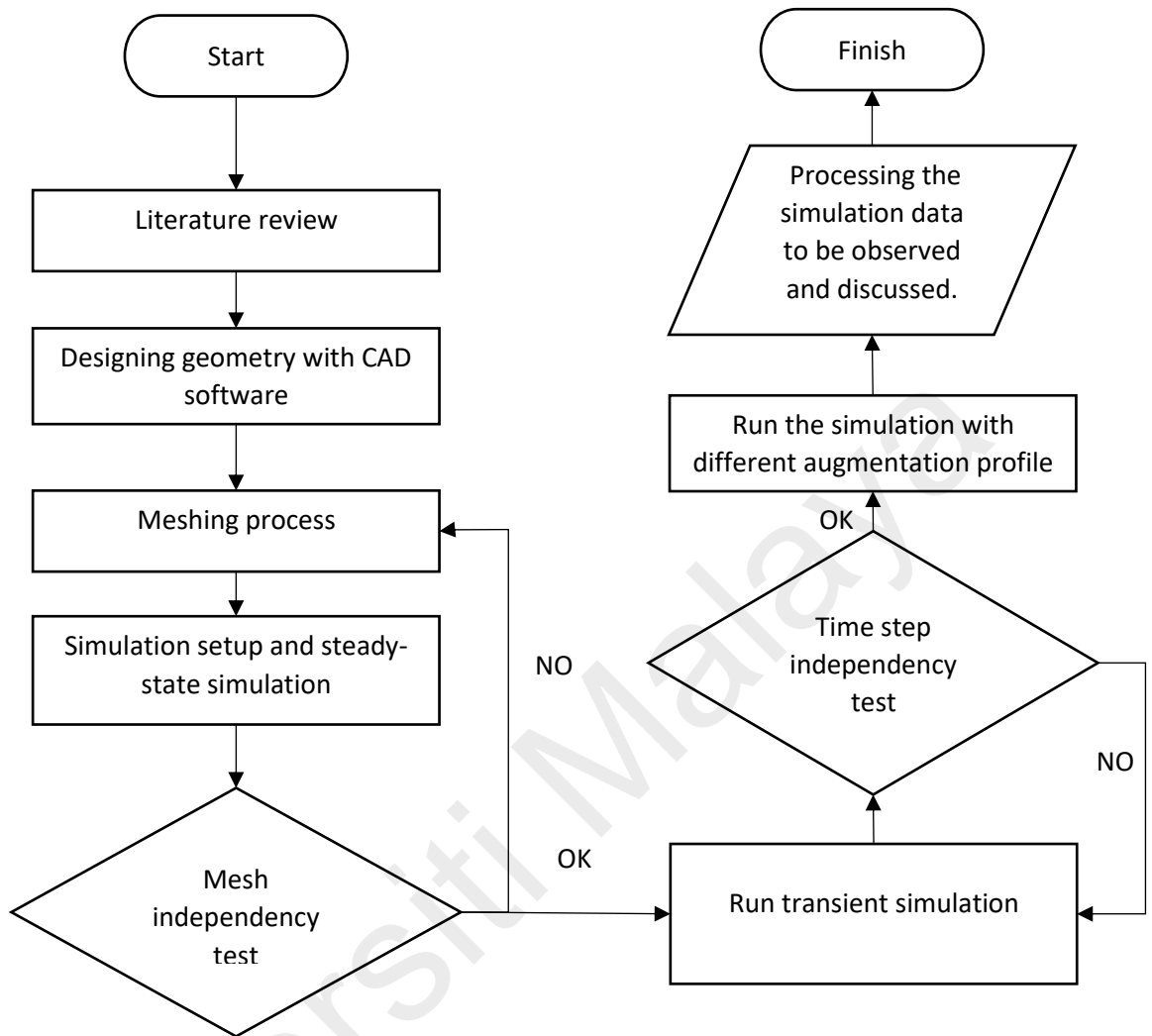


Figure 3.3: Numerical method flow chart

For this research, ANSYS™ Fluent® will be used to do the numerical method. This software uses the finite volume method to solve the Navier-Stokes equation, as seen in Eq. (3.1 – 3.3). This method will solve the governing equation by splitting the computational domain into smaller domains, usually called cells. Later, the Navier-Stokes equation is solved in each cell to obtain the value across the whole computational field.

Continuity :

$$\frac{\partial x}{\partial t} + \nabla \cdot (\rho \mathbf{u}) \quad (3.1)$$

$$\begin{aligned}
 \text{Strem} & : \rho \left(\frac{\partial u_x}{\partial t} + u_x \frac{\partial u_x}{\partial x} + u_y \frac{\partial u_x}{\partial t} \right) \\
 \text{function} & : = -\frac{\partial p}{\partial t} + \mu \left(\frac{\partial^2 u_x}{\partial x^2} + \frac{\partial^2 u_x}{\partial y^2} \right) + \rho g_x
 \end{aligned} \tag{3.2}$$

$$\begin{aligned}
 & : \rho \left(\frac{\partial u_y}{\partial t} + u_x \frac{\partial u_y}{\partial x} + u_y \frac{\partial u_y}{\partial t} \right) \\
 & : = -\frac{\partial p}{\partial t} + \mu \left(\frac{\partial^2 u_y}{\partial x^2} + \frac{\partial^2 u_y}{\partial y^2} \right) + \rho g_y
 \end{aligned} \tag{3.3}$$

The flowchart for this method can be seen in Fig. 3.3. This method has three main components, such as pre-processing, simulation, and post-processing setup. First, pre-processing involves creating the computer-aided design (CAD) geometry and meshing process. In this research, the CAD software used is Design Modeler that is available in ANSYSTM Workbench. The completed CAD geometry and dimensions for simulation can be seen in Fig. 3.4 and Table 3.1.

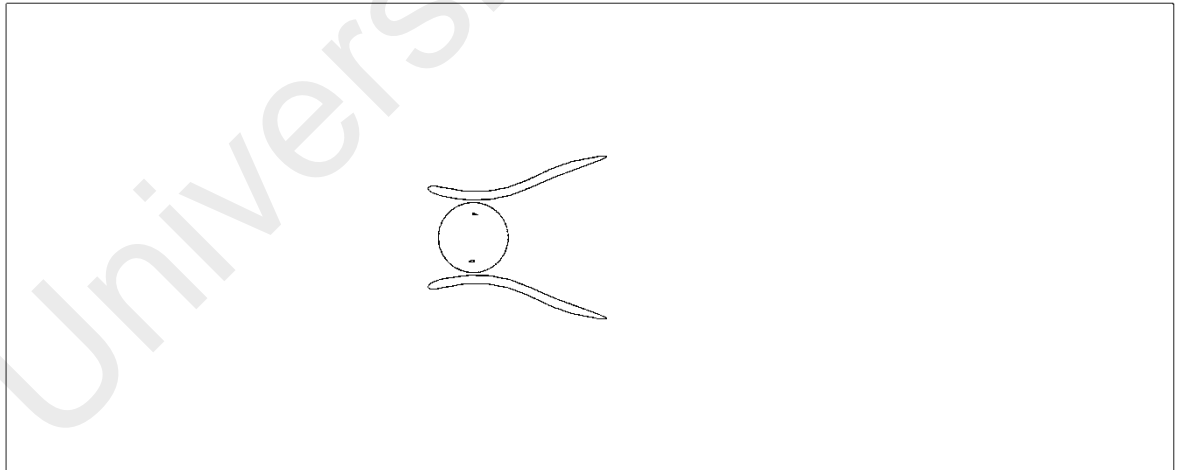


Figure 3.4: Visualization of the CAD used

The complete geometry can be imported into meshing software. The meshing process is carried out to divide the geometry into smaller sections called elements. The more number of elements, the solution will be as accurate as of the actual value. However, the more number elements generated by the meshing process will impact the computational

works, making it take longer to finish the simulation. Hence, it is crucial to do mesh independence to find the optimal number of elements to achieve efficient simulation time and accurate simulation data. In the meshing process, it is also essential to give a named selection to the geometry, which later will be a boundary condition, such as inlet and outlet. If the name selection is not carried out, the geometry will be considered as a wall.

Table 3.1: Validation geometry dimensions

Parameters	Specification
Diameter of Rotor	2000 mm
Pitch Angle (β)	6°
Chord Length	265 mm
Blade Profile	NACA0021
Rotating Zone	3000 mm
Box Size	50 m x 20 m
Rotor Distance	20 m

In the meshing process, an independent mesh test is crucial. Mesh independence is a process of finding the optimal number of elements by observing one or more parameters from the simulation data and comparing them with other different numbers of elements. Richardson's extrapolation or Grid Convergence Index (GCI) analysis method can be used to perform a mesh independence test (Phillips & Roy, 2014). When one or more parameters from the simulation data have a difference of around 1% between the mesh, it can be concluded that the mesh is already independent or does not affect the solution value too broad anymore.

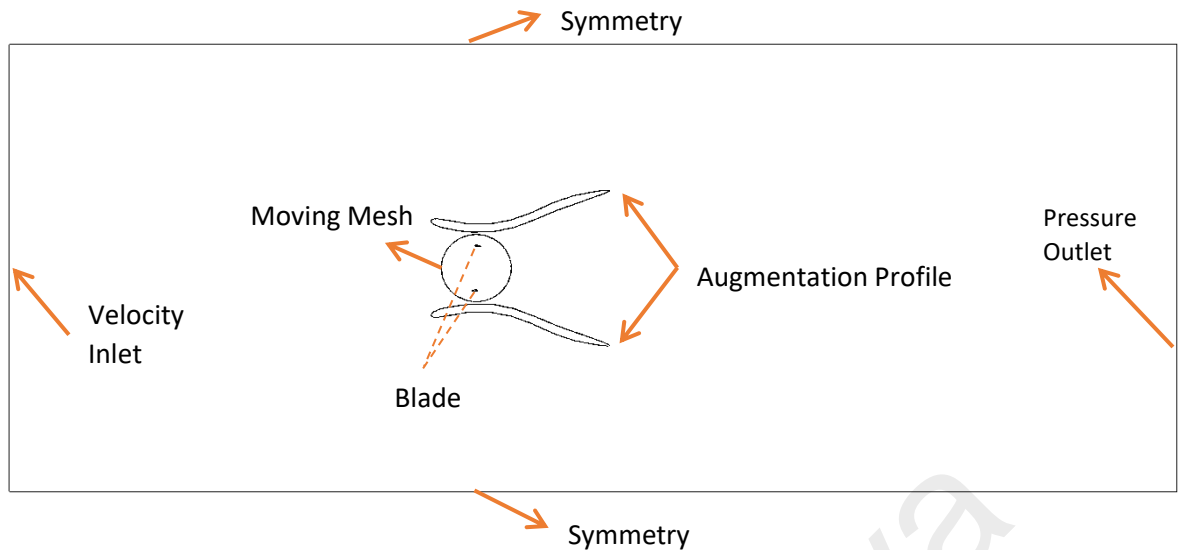


Figure 3.5: Visualization of the boundary condition

After the meshing process is done, the simulation setup can proceed. In the simulation setup, it is required to select the simulation condition that will be carried out for the numerical method. This research needs to do a numerical study with transient simulation. SST $k - \omega$ is chosen for the turbulence model in this research, which has good sensitivity in the boundary layer region. Since the augmentation will cause a boundary layer, SST $k - \omega$ is suitable for this research. The material properties used for this study are water with a density and viscosity of 998.2 kg/m^3 and 0.001003 kg/ms . The mesh motion is activated with a rotational speed, respectively changed according to the TSR value. For the validation case, the fluid used will be air with a TSR value of 2.58. The rotational speed of the mesh motion is calculated using Eq. (2.6), and the value is 20.64 rad/s . After that, the inlet boundary condition can be filled with a velocity inlet of 8 m/s , and initialization must be done before running the calculation. After the validation is done, the boundary condition is still the same as validation study. However, the value of the velocity inlet will be changed into 1 m/s . The gauge pressure outlet value is set into 0 Pa , which mean it is an atmospheric pressure condition. The overall simulation settings are concluded in Table 3.2.

Table 3.2: Numerical settings for this study

PARAMETERS	VALUE
TURBULENCE MODEL	$k - \omega$ SST
VELOCITY INLET	1 m/s
SOLUTION METHOD	second-order
PRESSURE OUTLET	0 Pa

Since this is a transient simulation, the time step independence test needs to be carried out. According to Maître et al., the minimum time step size used is a 2° rotation (Maître et al., 2013), so the time step independence test will be carried out between 0.5° , 1° , and 2° rotation. Fig. 3.5 shows the boundary conditions used for this research to visualize it easily. It can be seen in Fig. 3.5 that the augmentation profile is still a simple plate profile. Later in this research, the augmentation profile will be changed and improved to enhance the power coefficient further. The last step is post-processing, which analyzes the output parameter of the simulation. In this step, the flow characteristic and power coefficient can be observed.

CHAPTER 4: RESULT AND DISCUSSION

In this chapter, the analytical result and numerical result will be shown in this section. The analytical will consist of the calculation result of using the equation shown in chapter 3. The result will be compared to the numerical and validation work to see the differences between these methods. Next, using the numerical method, the outcome will consist of the mesh dependency, timestep dependency, validation, and power-augmented models. The result of both approaches will be observed, analyzed, and later be discussed with previous research that has been done. The power coefficient is the main output parameter that will be compared between the augmentation profiles. The flow behavior will be observed to know the reason for the power coefficient advancement of the augmentation profile.

4.1 Analytical Result

Equation (3.1 – 3.13) was used to produce the torque of the analytical method. The angle of attack (AOA) of the airfoil is changing every rotation. Thus, it was needed to calculate the AOA value on different azimuth angles. The angles used in this study have a difference of 10° . The AOA value will affect the C_L and C_D value, which will decide the torque. The value of the AOA can be seen in Table. 4.1.

Table 4.1: Angle of Attack value

Azimuth Angle ($^\circ$)	α (AOA)
0	-6
10	-3.211
20	-0.44981
30	2.255701
40	4.874257
50	7.37086
60	9.704766
70	11.82727
80	13.67895
90	15.18618
100	16.257

Azimuth Angle (°)	α (AOA)
110	16.77677
120	16.60481
130	21.57565
140	13.51213
150	10.263
160	5.777978
170	0.212596
180	-6

After calculating the value of AOA, the next step is to obtain the C_L and C_D value. These values can be obtained by doing a CFD steady simulation. However, in this study, open-source software will be used to get the C_L and C_D value on different AOA. *QBlade* is the software used to achieve the C_L and C_D data. This software does extrapolation of the airfoil generated or imported to 360° AOA data. These data will be used to calculate the torque, and the C_L and C_D graph can be seen in Fig. 4.1.

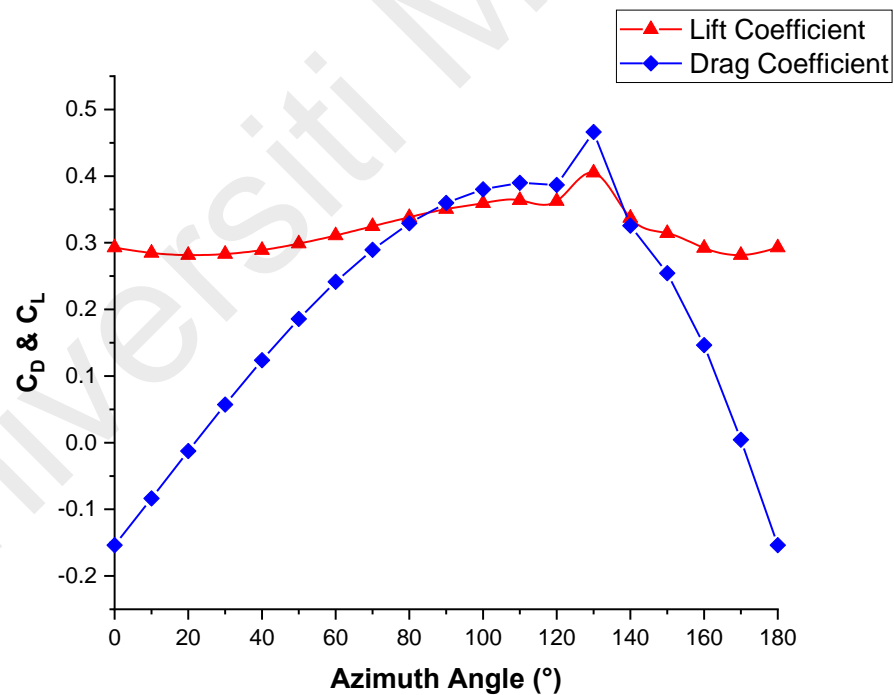


Figure 4.1: C_L and C_D graphic on different AOA

The data acquired from the *Qblade* will be used to calculate the torque and coefficient of torque of the airfoil NACA0021 blade. The result will be compared to Wong et al. study (Wong et al., 2018) and compared to the numerical validation method of this study. The data of the comparison can be seen in Fig. 4.2.

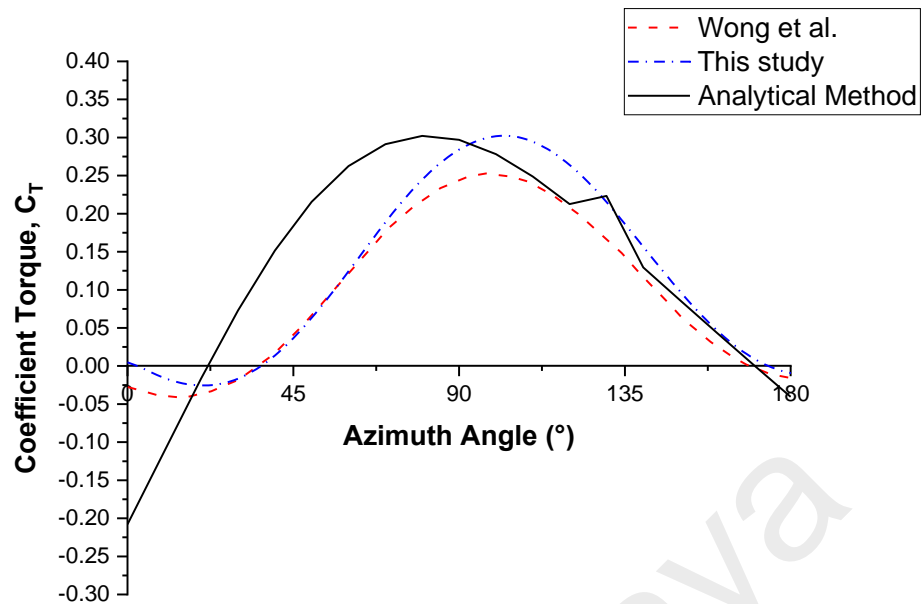


Figure 4.2: Analytical result of torque coefficient

As shown in Fig. 4.2, the analytical result is slightly higher than the numerical of Wong et al. The analytical result has a different peak value position than the numerical of Wong et al. The approximate analytical value is also achieved by calculating it every day 10° of azimuth angles. Every 10° difference of azimuth angle was chosen to calculate the analytical outcome quickly since this method approximates the blade's theoretical value for this study.

4.2 Dependency Result

The mesh dependency result is the foremost thing that needs to be done in the first place. The value of the mesh dependency can be seen in Table. 4.2. The mesh settings used for this study are decided with a 172941 number of elements. The inflation used is 0.17 mm first layer thickness with 15 layers to get an accurate result of the torque at the blade profile. Later, the inflation settings were applied to the augmentation profile to achieve a precise velocity value near the boundary.

Table 4.2: Mesh dependency result using Grid Convergence Index (GCI) analysis for the validation study

Number of Elements	Grid Spacing	r	Moment	p	GCI
49428	2.711865075	-	-2.21571	-	
172941	1.449791717	1.87052	-1.75794	-5.3468	26.7660145%
363504	1	1.449792	-1.74185	-9.01475	1.185667794%
Infinity	0		-1.72517		

The output parameter used to observed the mesh dependency test is the torque at the blade. The mesh dependency has an error of around 1% for this study. Richard's extrapolation results shown in Fig. 4.3 shows the different torque value in grid spacing or the number of elements. The result prediction using the extrapolation method should be around -1.725 Nm at infinite grid spacing or zero, which has a difference of about 1% from the previous grid spacing value. The mesh visualization can be seen in Fig. 4.4, used for further numerical study for the time step dependency test and validation work.

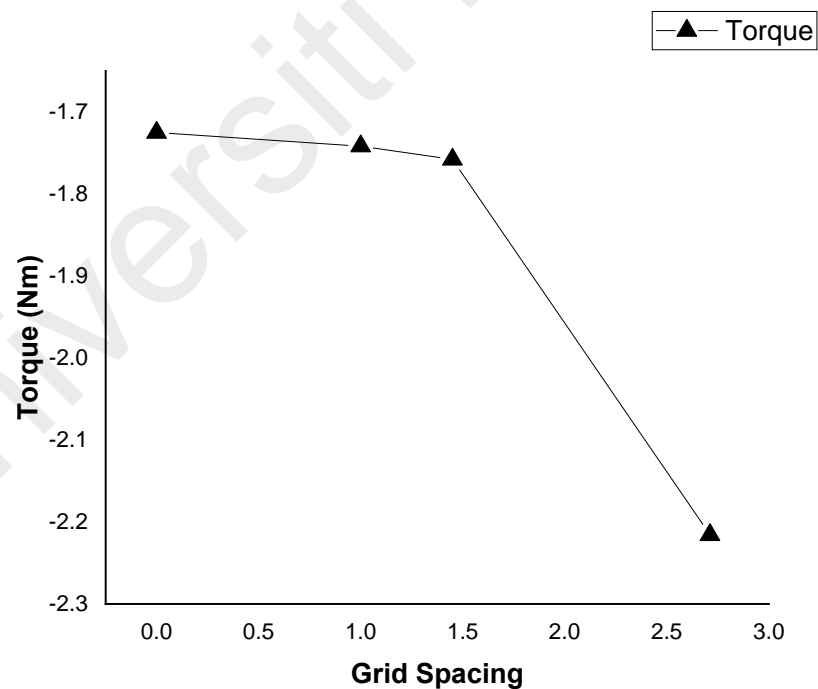


Figure 4.3: Torque value on a different grid spacing for the validation study

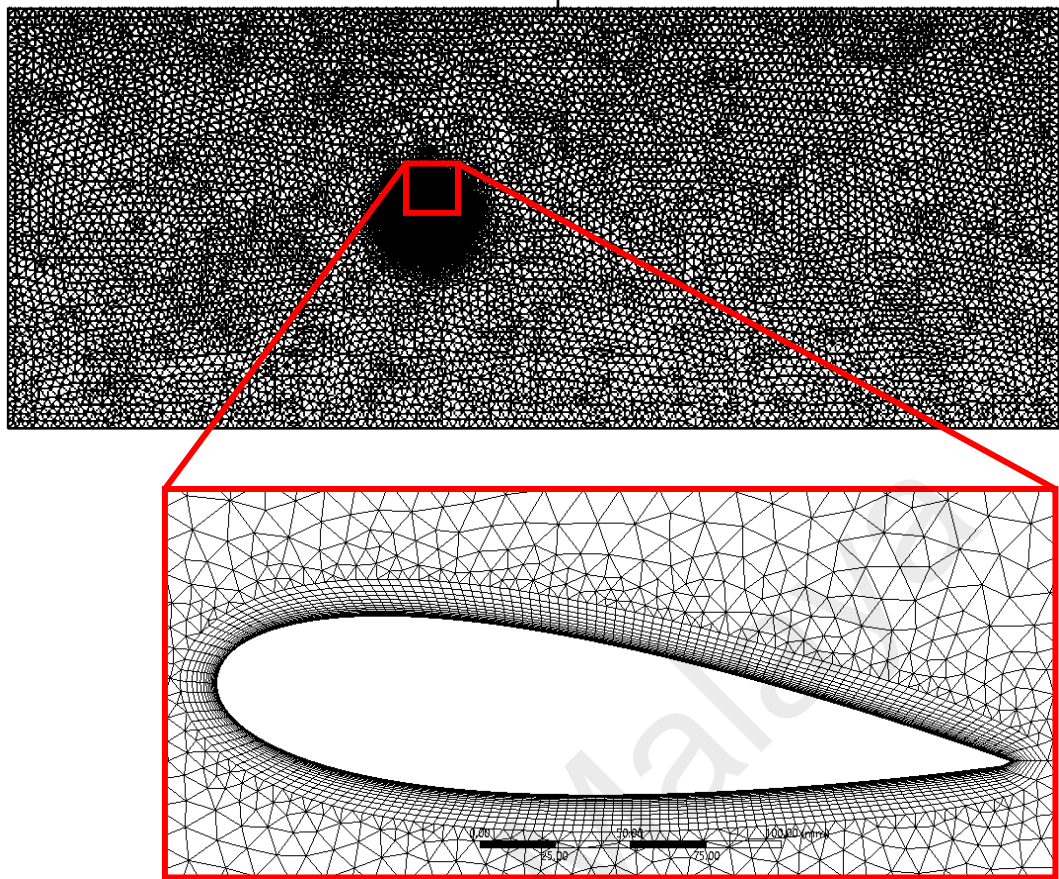


Figure 4.4: Visualization of mesh used for the validation study

After the mesh dependency result is good enough, the timestep dependency test will be carried out to determine how many degrees of rotation are needed for each time step for the numerical method of this study. This simulation will be using the validation geometry as well, so the validation is also done at the same time when the time step dependency result is obtained. As mentioned in the previous chapter, the time step dependency will be compared between 2° , 1° , and 0.5° rotation for every time step. The comparison result will be shown in Fig. 4.5, which shows that the influence of the three differences on the degree of rotation is very little, almost not noticeable. The 2° has a lower power coefficient than the other timestep. Thus, the 1° is chosen to keep the accuracy of the data, also reducing the computational speed.

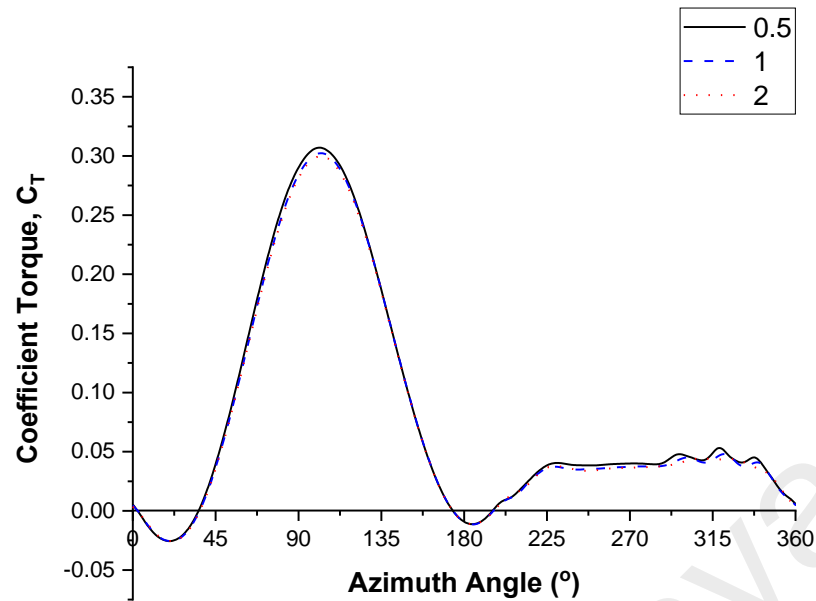


Figure 4.5: Timestep dependency result

4.3. Validation Result

The validation result is redoing Wong et al. numerical study (Wong et al., 2018). However, this study will be using a 2D method for the numerical. The 2D numerical method will be compared with the same geometry dimension and settings. The coefficient of torque of the blade will be used as an output parameter for this validation work. The simulation uses an air velocity of 8 m/s with SST $k - \omega$ turbulence model. The result of this validation will be shown in Fig. 4.6. It can be seen that the 2D numerical result is higher compared to the 3D numerical on the early azimuth angle. This result indicates that these two methods only have slight differences, which can be used to consider the outcome value for the further of this study. A drag and lift loss may occur a lot higher using a 3-dimension numerical method than a 2-dimension, which causes the overall torque and power coefficient to be lower in Wong et al. compared to this study.

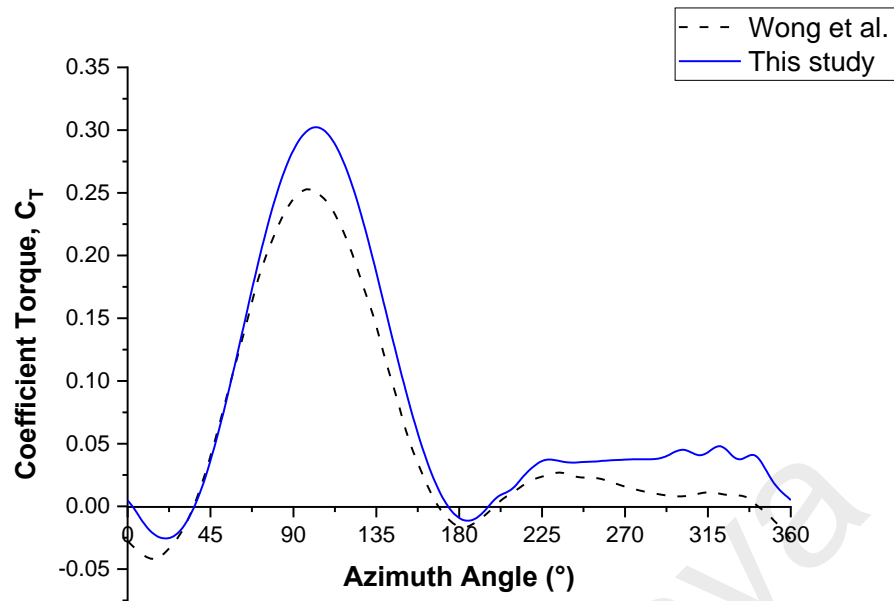


Figure 4.6: Comparison of torque coefficient for validation

4.4. Numerical Result

After the validation had been done, it is crucial to know the power curve of the water turbine that will be used for further improvement with augmentation. Because of that, the first thing that will be done is to do the simulation to achieve the turbine's power curve. The settings are similar to the validation works, although the fluid material needs to be changed into water. The water velocity of 1 m/s is used to do this study. According to Saupi et al. study (Saupi et al., 2018), the river's speed can reach up to 2 m/s or more. Thus, the value of 1 m/s was chosen to consider the performance of the hydrokinetic turbine at a low current speed. This simulation used five different TSR values, 2.0, 2.58, 3.0, and 3.5, to produce the power curve graph. The result is shown in Fig. 4.7.

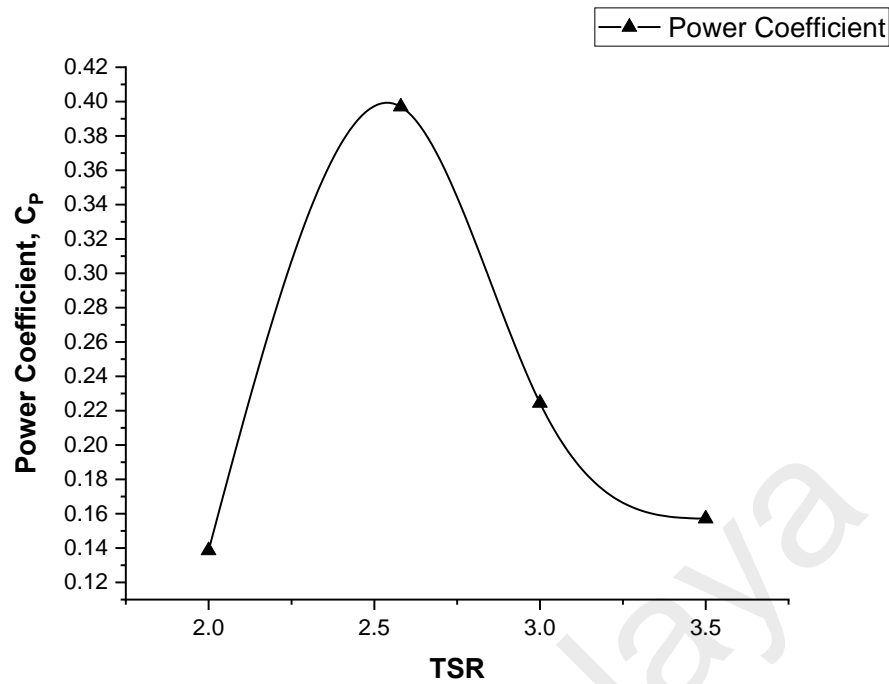


Figure 4.7: Power curve of the NACA0021 blade used in this study

It can be seen from Fig. 4.7 that the highest power coefficient occurs when TSR is equal to 2.58, with a value of 0.397. It appears that the power coefficient is high enough for this turbine. However, augmentation can be used to enhance further the power coefficient to achieve a higher power coefficient. First, a flat plate augmentation profile will be used to observe the significance of the venturi effect on the power coefficient. Later, a better airfoil profile will be used for the augmentation to minimize the geometry size, which will have a better performance increase.

4.4.1. Flat Plate Augmentation Profile

The first thing this study tried to enhance the capability of the turbine to harness the energy from the river is using a flat plate as the augmentation. It is a typical shape that is easy to build and manufactured. The purpose of choosing a flat plate is to prove the venturi effect, mainly caused by the ratio of the inlet and outlet of the augmentation. The flat plate geometry used has 6500 mm in length with a thickness of 100 mm, and the visualization can be seen in Fig. 4.8.

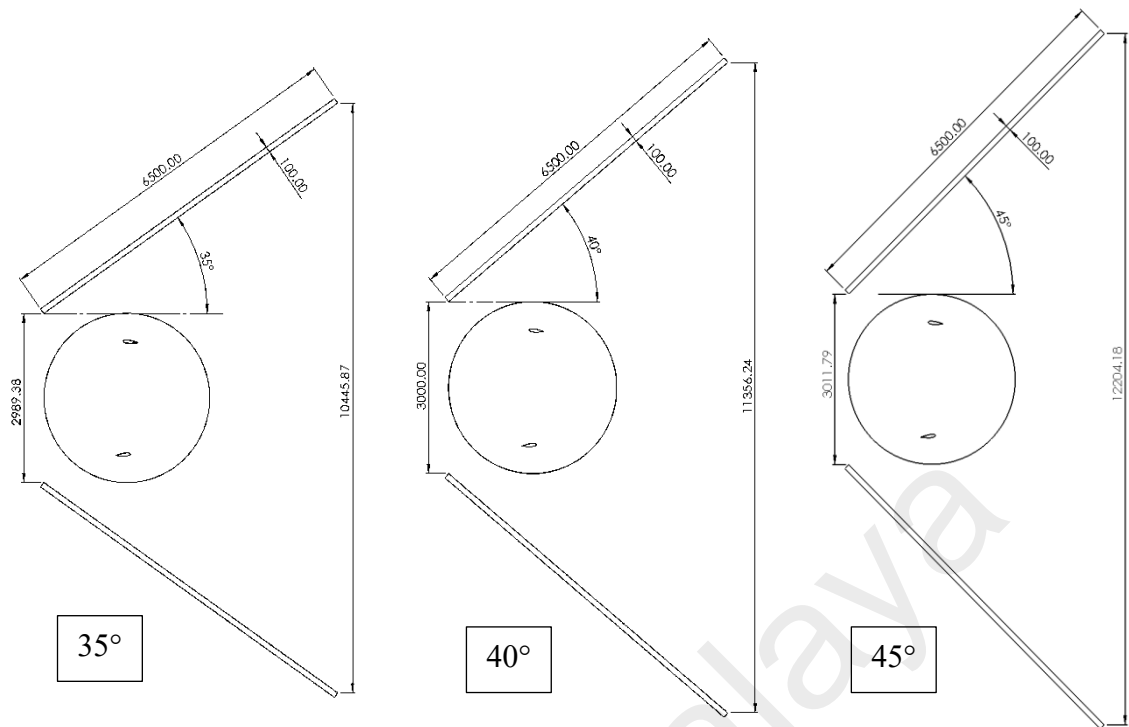


Figure 4.8: Three different flat plate augmentation profiles

Three different angles of the flat plate will be observed. The flat plate angles are 35° , 40° , and 45° . The flat plate opening is fixed, so when the slopes are steeper, the outlet of the augmentation is getting bigger, making the ratio between them increase. The numerical simulation is first done in steady-state conditions to observed the flow behavior caused by the flat plate. The result of the steady-state simulation can be seen in Fig. 4.9.

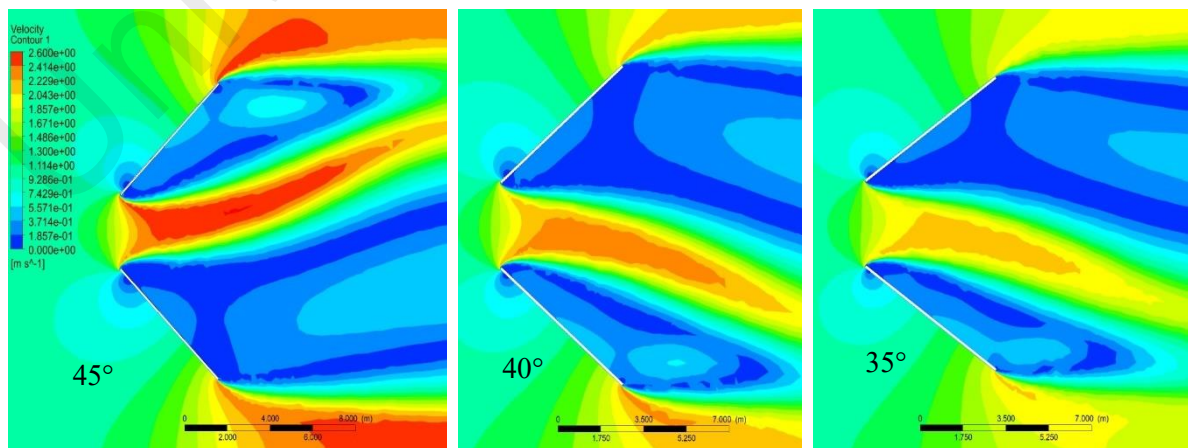


Figure 4.9: Velocity contour of steady-state simulation on flat plate augmentation

From the steady-state simulation, the enhancement in the velocity is very significant. The 45° flat plate has the most outstanding improvement from 1 m/s to a speed of around 2.6 m/s. Since the steady-state simulation has been done and observed, the transient simulation will now be executed to keep the turbine's behavior with the flat plate. The transient simulation is carried out with a TSR value of 2.58. This value was chosen because it has the highest power coefficient from the bare turbine power curve simulation. The coefficient of power result shown in Fig. 4.10 indicates that the torque rippling happens so great. Although it looks like the power coefficient is very high, the highest average power coefficient is 0.749 by 45° flat plate. The improvement of the power coefficient is not that significant from the 40° flat plate to the 45°. The 40° achieved power coefficient of 0.718, and the smallest power coefficient achieved by the 35° with a power coefficient of 0.563.

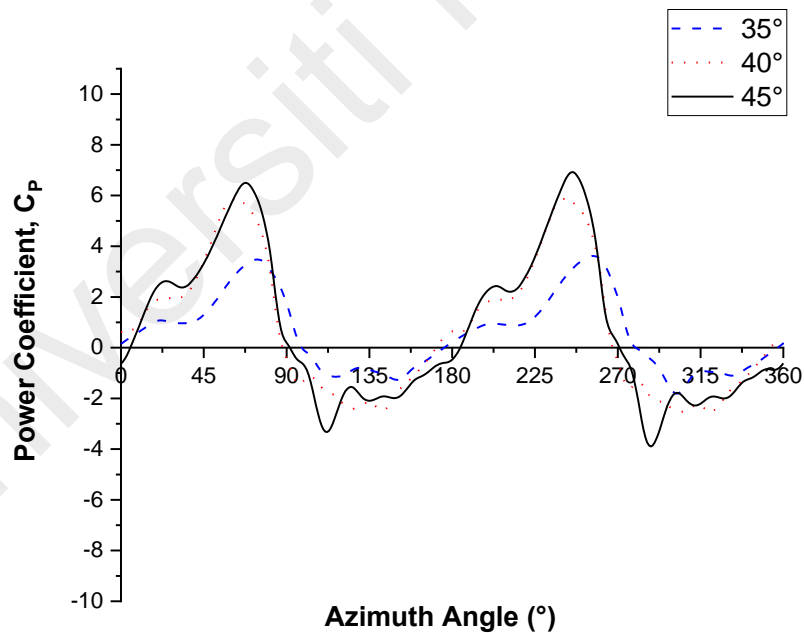


Figure 4.10: Flat plate power coefficient for one revolution at TSR is equal to 2.58

4.4.2. Airfoil Augmentation Profile

Since the geometry CAD model is slightly different from the previous one, another mesh dependency test is carried out to find the augmentation's optimal meshing size.

Previous mesh settings are used, and the mesh dependency test is carried out only for finding the optimal meshing setting for the augmentation model. The GCI analysis can be seen in Table 4.3, and Richardson's extrapolation value will be shown in Fig. 4.11. The mesh sizing of the augmentation is 15 mm with first-layer thickness inflation of 0.5 mm, and 15 layers are used.

Table 4.3: Mesh dependency result using Grid Convergence Index (GCI) analysis for the augmentation study

Number of Elements	Grid Spacing	r	Moment	p	GCI
122679	2.047155585	-	-9.70849	-	
179913	1.39591358	1.466535	-10.2763	-6.7261	7.912359%
251143	1	1.395914	-10.3195	-7.72132	0.569016%
Infinity	0		-10.2727		

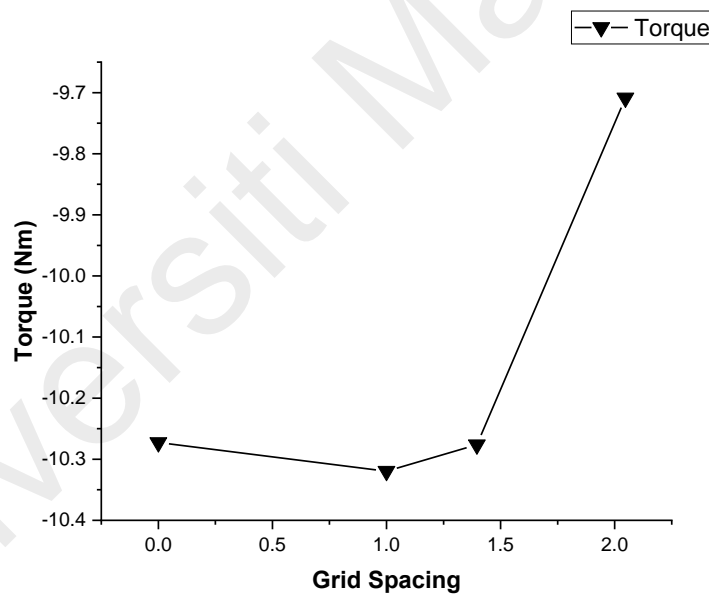


Figure 4.11: Torque value on a different grid spacing for augmentation study

Although using a 45° flat plate can achieve a high power coefficient, it is not feasible to implement it in the river since there is insufficient space. Thus, another type of augmentation profile that has a lower space consumption needs to be implemented. An airfoil profile will be developed to enhance the flow to obtain a better power coefficient with minimal space usage. The space usage of this augmentation is similar to a 35° flat plate with a value of 0.563. Because of that, the power coefficient of the airfoil

augmentation profile will be compared to a 35° flat plate result. The airfoil profile used for the augmentation is NACA0015 with a chord length of 2000 mm. The visualization of the airfoil augmentation profile can be seen in Fig. 4.12.

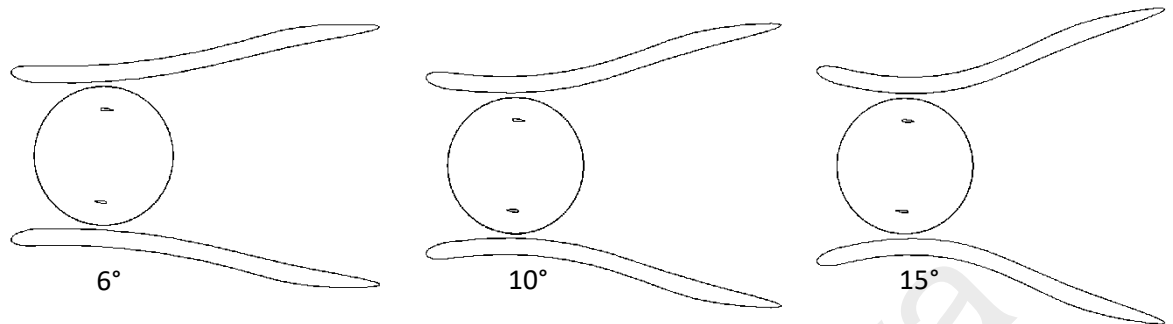


Figure 4.12: Three different geometry of an airfoil augmentation

Three models with different pitch angle variations of 6°, 10°, and 15° were used for this observation. The observation will be done in steady-state first to look at the velocity enhancement caused by the models. Later, the velocity contour result can be seen in Fig 4.13, showing that the velocity is more stable than a flat plate.

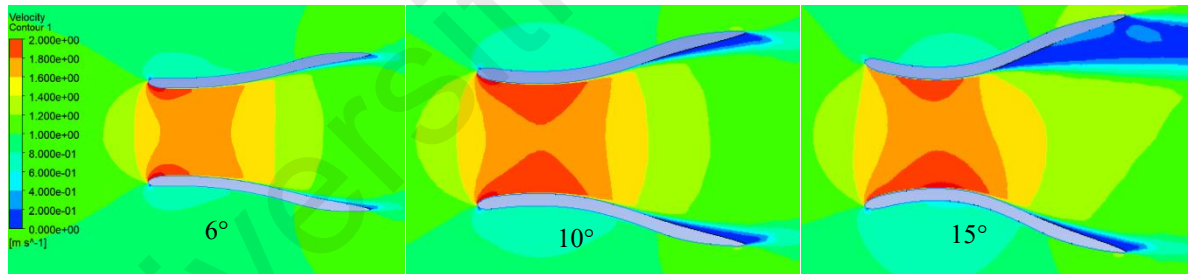


Figure 4.13: Velocity contour on the airfoil augmentation profile

The velocity contour shows that an airfoil augmentation achieves the highest uniform velocity profile with a 10° pitch angle. It has been observed already in flat plate augmentation that higher velocity means higher kinetic energy available. From the previous observation with the flat plate, it can be hypothesized that the better velocity will achieve a better power coefficient.

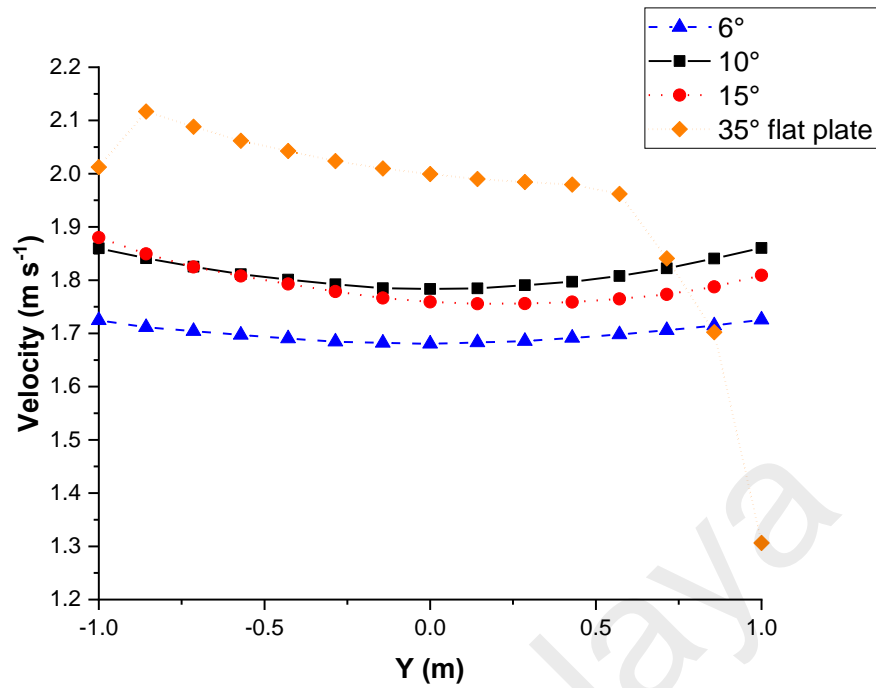


Figure 4.14: Velocity value on Y-axis location of different augmentation profiles

After the steady-state simulation has been observed and analyzed, a transient simulation with the turbine blade will be carried out. The same as the flat plate transient simulation, a TSR of 2.58 was chosen for this study. The power coefficient of the three augmentation profiles is shown in Fig. 4.15. From the graphic, it can be seen that the ripple is not as worse as using the flat plate. From Fig. 4.15, it appears that the higher velocity contour does not mean better performance. The 6° airfoil profile achieved the highest performance with a power coefficient of 0.614. The 10° and 15° do increase the power coefficient, reaching 0.476 and 0.454, respectively. It can be seen that the highest performance achieved by 6° airfoil profile, which caused by the changing in the velocity vector before hitting the turbine's blade. The angle is the same between the pitch angle at the turbine's blade and the augmentation profile, which can cause the significance enhancement by this augmentation profile. The power coefficient in a complete revolution will be observed in Fig. 4.15.

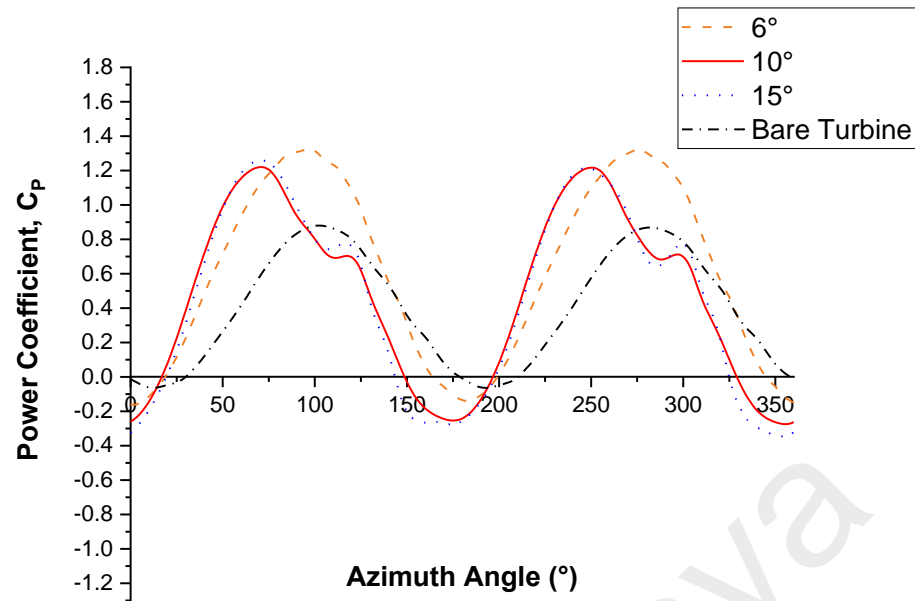


Figure 4.15: Power coefficient of different airfoil augmentation profiles at TSR is equal to 2.58

Fig 4.15 also indicates the negative value is higher compared to the bare turbine. The 10° and 15° have a lower power coefficient because of the negative torque produced by the turbine. This phenomenon also happens to flat plate augmentation. The blade makes a high value of negative torque, reducing the performance of the turbine. The torque of the blade will be compared to look at the negative torque produced by a different type of airfoil augmentation to observe this phenomenon better. Fig 4.16 will show the torque comparison between these three airfoil augmentation profiles. It can be seen that although the torque is slightly higher, the negative torque is produced by the blade after 250° of

azimuth angle also higher, which makes the performance worse. There are two blades in the turbine, creating the effect twice worse.

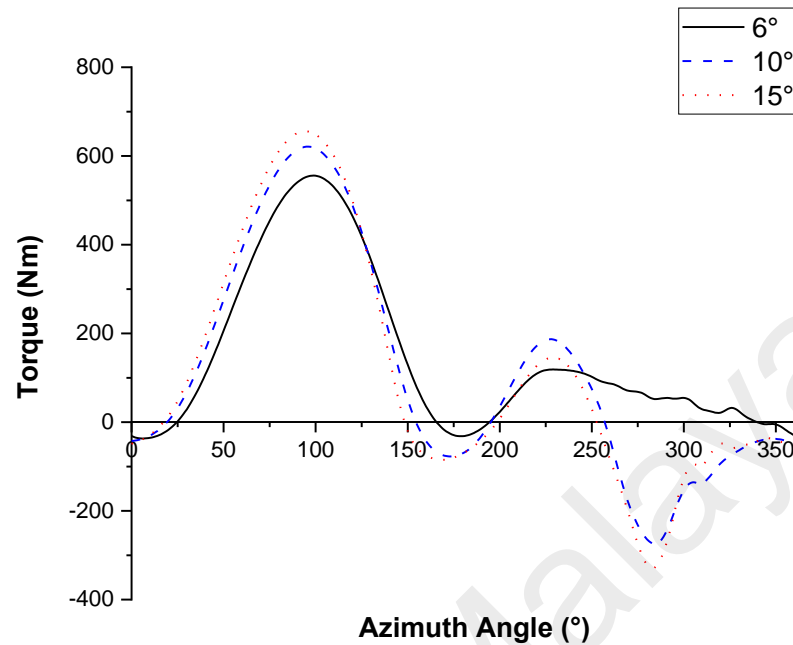


Figure 4.16: Torque value comparison between different airfoil augmentation profiles

The velocity contour can be compared around the azimuth angle of 280° to observe the negative torque generation. Fig. 4.17 compares the velocity contour of the 6° and 10° augmentation profiles. From Fig. 4.17, it can be seen the wakes generation at the blade around that region is higher at 10° compared to the 6° . This wake generation is causing the torque to have a negative value. The wake itself generates because of the vector changed by the augmentation profile, making the velocity vector hitting the blade at that region change. Thus, the negative torque produces by the airfoil blade in this region of the turbine.

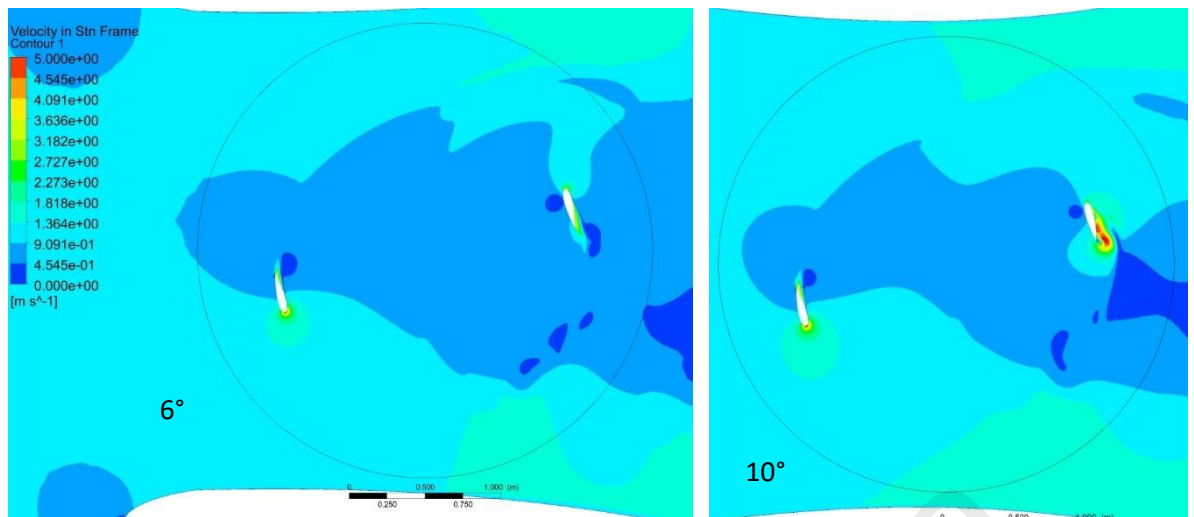


Figure 4.17: Velocity in the stationary frame comparison of 6° and 10° airfoil augmentation profiles

The flow behavior had been observed, and the augmentation profile affects the velocity vector causing wake generation. Thus, observation of the turbine's power curve with the 6° augmentation profile will be carried out. This observation analyzes whether the optimum rotational speed or tip speed ratio value of the turbine changed when installing the augmentation. Fig 4.18 shows that the optimum power coefficient is achieved at the TSR value of 3.0. The power coefficient reached 0.704, which means the power-augmentation model could produce a 77.33% enhancement of the turbine's performance. From Fig 4.18, it appears that the turbine power curve shows a better overall performance with augmentation. At the TSR value of 3.5, the power coefficient of the turbine has not fallen out drastically compared to a bare turbine. The power coefficient only dropped from 0.704 to 0.688 at the TSR of 3.5. It shows that with augmentation, the working condition coverage a load border compared to the bare turbine. It is a tremendous improvement because, in the actual condition, the hydrokinetic turbine might work at different values of TSR caused by the river condition.

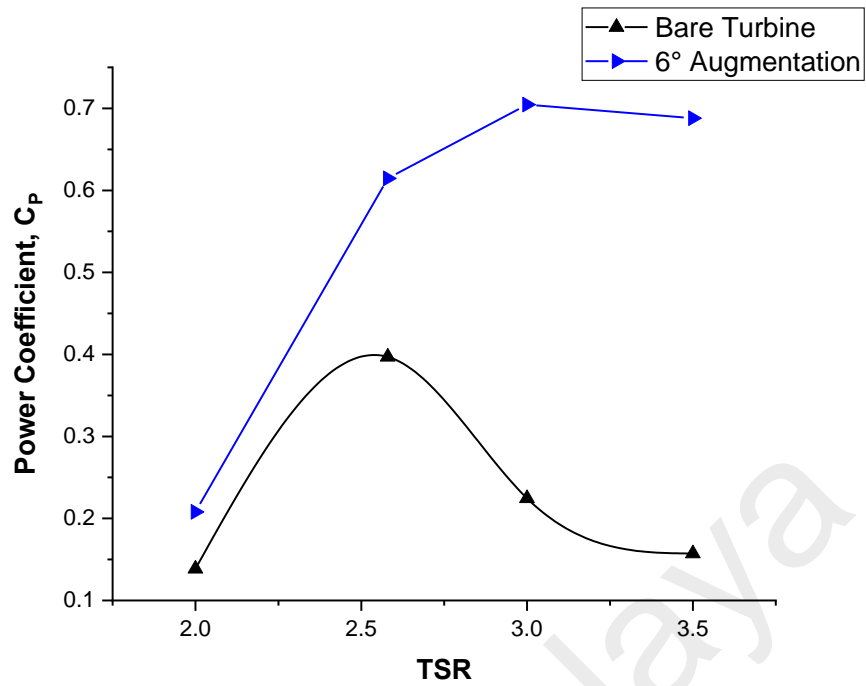


Figure 4.18: Power curve comparison of the airfoil augmentation and bare turbine

The flow behavior had been observed, and the augmentation profile affects the velocity vector causing wake generation. In addition, another observation of the rotor distance or positioning will be carried out. This observation was done to make sure the position of the rotor place optimally with the augmentation. Changing the positioning of the turbine affects both the velocity magnitude and vector when hitting the blade. The dimensionless parameter of rotor diameter (D) over the position distance (ΔX) will be used to observe the power coefficient differences. A dimensionless parameter is used because it will be easier if a scaling wants to be carried out for further research or implementation in the river. The visualization of the dimensionless parameter will be shown in Fig. 4.19.

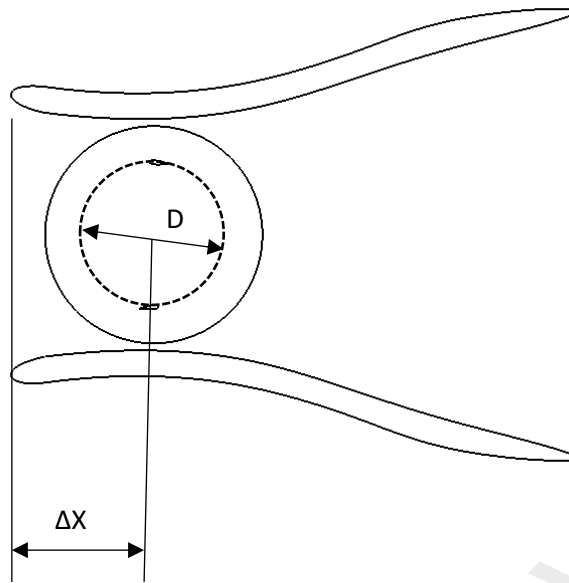


Figure 4.19: Visualization of the dimensionless parameter

This observation will be carried out only with the best airfoil profile, the 6° augmentation profile. Three values of the dimensionless parameter will be used in this observation, 1.0, 1.25, and 1.67. The testing will be done with the best TSR value at 3.0 of the 6° augmentation profile. The output parameter that will be observed is the average power coefficient of the turbine. The outcome of the rotor positioning in the augmentation will be shown in Fig. 4.20. The power coefficient slightly increases when the dimensionless parameter value of 1.2 has a power coefficient value of 0.712. However, the power coefficient dropped drastically when the diameter ratio over the rotor placement distance is 1.67 with a power coefficient value of 0.28.

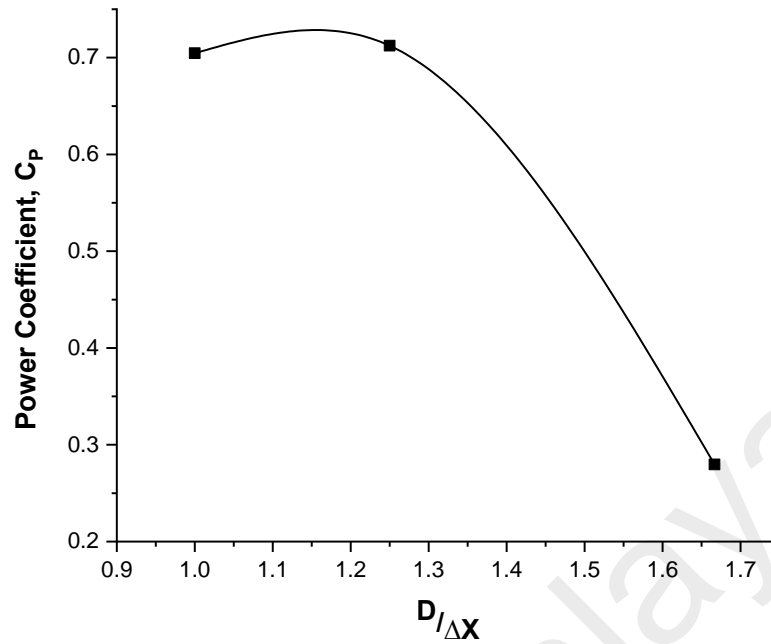


Figure 4.20: Power coefficient of 6° airfoil augmentation in a different position

4.4 Discussion

This study proves that the venturi effect enhances the velocity stream, which significantly affects the power coefficient. This result is verified with a lot of the previous research, which also improves the performance. In Malipeddi et al.'s study, the ducting shape can increase the power coefficient to 0.63 from 0.40 (Malipeddi & Chatterjee, 2012). Elbatran et al. research also achieved a 70% performance enhancement by installing a diffuser (Elbatran et al., 2016).

The ducting profile of their research can be seen in Fig. 4.21. Malipeddi et al. also do a turbine positioning when installing the duct. Their study achieved when the turbine is moved 0.4 m, the power coefficient slightly increases from 0.63 to 0.644. This result is very similar to this research, which barely enhances the power coefficient from 0.704 to 0.712 when the turbine position changes slightly.

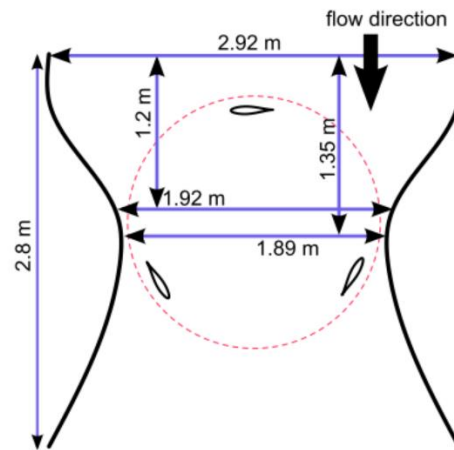


Figure 4.21: Duct geometry used in Malipeddi study (Malipeddi & Chatterjee, 2012)

Malipeddi et al.'s research also do an external shape configuration, making the turbine's better performance. The power coefficient reached 0.72 with a design of an outer shape called E2 shown in Fig. 4.22. The enhancement effect from the ducted design of their study is on par with this current research with the airfoil augmentation profile. However, the blade configuration used for this research is not optimum. Thus, when the blade configuration is changed into a better one. The airfoil profile configuration will be better than Malipeddi's ducted structure.

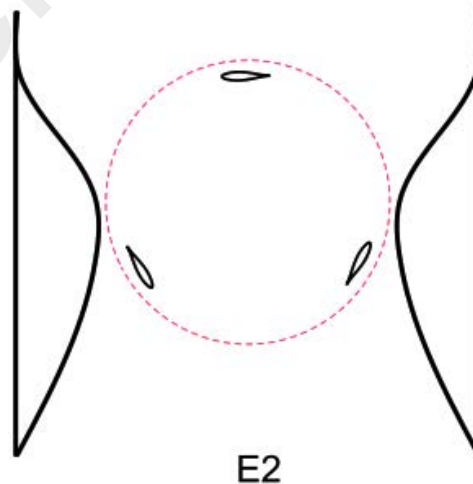


Figure 4.22: External shape design in Malipeddi study (Malipeddi & Chatterjee, 2012)

The current research's result is arguing the Barbarić & Guzović research, which shows only a 40% enhancement of the performance using airfoil profile for their diffuser (Barbarić & Guzović, 2020). Although the airfoil design is different from the current study, it is proved that it can reach higher with an airfoil profile than using a flat plate augmentation. A 77.33% enhancement of the power coefficient was achieved in this research using an airfoil profile augmentation.

There are also many better results of augmentation profile such as Roa et al. study (Roa et al., 2010) and Rezek et al. study (Rezek et al., 2021). Both of these research achieved a power coefficient of more than one after installing a diffuser for augmentation. Diffuser augmentation can accomplish more than one power coefficient since a horizontal axis is used for the turbine. Compared to a vertical axis turbine, a horizontal axis turbine won't have a negative torque ripple even after installing the diffuser. However, this research's findings are that with the correct augmentation profile structure for a vertical-axis turbine, a torque ripple can be minimized and still increasing the power coefficient significantly. The 6° airfoil augmentation profile can achieve minimal negative torque with a significant enhancement of the torque, which substantially improves the power coefficient of the turbine.

From the flat plate observation, the bigger the augmentation's opening, the better velocity magnitude it can achieve. Thus, advance improvement can be made if there is any space available to install the augmentation. The edge of the end of the 6° augmentation profile can be bend more outward to have a better velocity magnitude without changing the velocity vector when hitting the blade. The power coefficient surely will improve if there is more space available on the site.

CHAPTER 5: CONCLUSION AND FUTURE WORK

5.1 Conclusion

This study data is achieved by performing computational fluid dynamics simulation, validated or verified using previous research. The hydrokinetic turbine used in this study is a two-blade vertical-axis type with a symmetrical airfoil NACA0018. The turbine achieved the highest power coefficient of 0.39 at TSR is equal to 2.58. Furthermore, this study analyzed an augmentation profile to improve the turbine performance. A preliminary study on a flat plate profile is used for the augmentation. Three different flat plates with different angles are observed. A venturi's effect can be seen caused by the structure of the augmented profile. The velocity increases twice from the freestream velocity on this flat plate study. The ratio of the inlet and the outlet of the augmentation was the factor of improving the speed. The improvement of the velocity will affect the performance of the turbine. The 35°, 40°, and 45° flat plate augmentation achieved a power coefficient of 0.563, 0.718, and 0.749, respectively.

However, higher flat plate angles mean a higher space required. Thus, a better-augmented geometry profile was observed to achieved better performance with minimum space required. An airfoil augmentation was designed with three different pitch angles use for developing the geometry. A NACA0015 was used for the airfoil augmentation with 6°, 10°, and 15° pitch angles. The airfoil design is compared to the 35° flat plate model since the ratio of the inlet to outlet of the augmentation is similar. The velocity improvement is lower than the flat plate augmentation than the 35° flat plate design. Although the velocity improvement is more insufficient than the flat plate design, the performance improvement is more significant than the flat plate design. The 6° airfoil augmentation achieved the most remarkable development with a power coefficient value of 0.704, although the 10° and 15° airfoil profiles have a better velocity improvement

than the 6°. The 10° and 15° augmentation designs only achieved 0.476 and 0.454 power coefficients, respectively.

This study shows that the 6° airfoil augmentation can improve 77.33% performance. However, the turbine positioning has not been analyzed whether the initial placement can achieve the best power coefficient or not. Therefore, an observation was carried out and found that the performance increase slightly, which improve the turbine as high as 79.34%. This airfoil augmentation is far better compared to the flat plate design.

5.2 Future Work

This study can be further advanced from the blade selection aspect, another airfoil profile for the augmentation, and experimental prototyping and testing. A better type of airfoil blade can be used to improve the turbine performance more. An optimum number of blades can be observed to see whether there is a significant impact after augmentation has been applied to the turbine. Another airfoil profile also needs to be investigated for the augmentation structure. This study only uses NACA0018 with a specific chord length of 2000 mm with different pitch angles. Another airfoil profile might be able to produce better enhancement for the hydrokinetic turbine.

The most important thing that needs to be done is test the CFD result with water tunnel testing. A prototype needs to be manufactured and tested to validate the findings of this study further. A water tunnel or another testing method will significantly validate this work, making these findings more impactful. After it has been tested, the result of this study can be fully implemented for rural area development to utilize hydropower from a river.

REFERENCES

- Administration, U. S. E. I. (2020). *U. S. Energy-Related Carbon Dioxide Emissions*, 2019. September.
- Bachant, P., & Wosnik, M. (2015). Performance measurements of cylindrical- and spherical-helical cross-flow marine hydrokinetic turbines, with estimates of exergy efficiency. *Renewable Energy*, 74, 318–325.
<https://doi.org/10.1016/j.renene.2014.07.049>
- Bank, A. D., Economic, U. N., & Commission, S. (2019). *Renewable Energy Status Report*.
- Barbarić, M., & Guzović, Z. (2020). Investigation of the possibilities to improve hydrodynamic performances of micro-hydrokinetic turbines. *Energies*, 13(17).
<https://doi.org/10.3390/en13174560>
- Benchikh Le Hocine, A. E., Jay Lacey, R. W., & Poncet, S. (2019). Multiphase modeling of the free surface flow through a Darrieus horizontal axis shallow-water turbine. *Renewable Energy*, 143, 1890–1901.
<https://doi.org/10.1016/j.renene.2019.06.010>
- Carlton, J. S. (2012). The Propeller Environment. *Marine Propellers and Propulsion*, 47–56. <https://doi.org/10.1016/b978-0-08-097123-0.00004-6>
- Daniele, E., & Coiro, D. P. (2013). Optimization of diffuser geometry for an horizontal axis shrouded hydro turbine. *4th International Conference on Clean Electrical Power: Renewable Energy Resources Impact, ICCEP 2013, January 2018*, 240–247. <https://doi.org/10.1109/ICCEP.2013.6586996>
- Davidson, L. (2015). *Fluid mechanics, turbulent flow and turbulence modeling*. Chalmers University of Technology.
- ed-Dîn Fertahi, S., Bouhal, T., Rajad, O., Kousksou, T., Arid, A., El Rhafiki, T., Jamil, A., & Benbassou, A. (2018). CFD performance enhancement of a low cut-in speed current Vertical Tidal Turbine through the nested hybridization of Savonius and Darrieus. *Energy Conversion and Management*, 169(February), 266–278.
<https://doi.org/10.1016/j.enconman.2018.05.027>
- Elbatran, A. H. A., Yaakob, O. B., Ahmed, Y. M., & Abdullah, F. B. (2016). Augmented diffuser for horizontal axis marine current turbine. *International Journal of Power Electronics and Drive Systems*, 7(1), 235–245.
<https://doi.org/10.11591/ijpeds.v7.i1.pp235-245>
- Fleisinger, M., Vesenjajk, M., & Hriberšek, M. (2014). Flow driven analysis of a darrieus water turbine. *Strojniski Vestnik/Journal of Mechanical Engineering*,

- Fouladi Fard, R., Naddafi, K., Yunesian, M., Nabizadeh Nodehi, R., Dehghani, M. H., & Hassanvand, M. S. (2016). The assessment of health impacts and external costs of natural gas-fired power plant of Qom. *Environmental Science and Pollution Research*, 23(20), 20922–20936. <https://doi.org/10.1007/s11356-016-7258-0>
- Han, D., Heo, Y. G., Choi, N. J., Nam, S. H., Choi, K. H., & Kim, K. C. (2018). Design, fabrication, and performance test of a 100-W helical-blade vertical-axis wind turbine at low tip-speed ratio. *Energies*, 11(6), 1–17. <https://doi.org/10.3390/en11061517>
- Ho-Yan, B. (2012). *Design of a low head pico hydro turbine for rural electrification in Cameroon*. <http://atrium.lib.uoguelph.ca/xmlui/handle/10214/3552>
- Holt, A., & Pengelly, I. J. (2008). ITS and renewable energy. *15th World Congress on Intelligent Transport Systems and ITS America Annual Meeting 2008*, 6, 3854–3862. <https://doi.org/10.1049/ic.2008.0789>
- International Energy Agency. (2021). *World Energy Model 2020* (Issue February).
- Khan, M. J., Bhuyan, G., Iqbal, M. T., & Quaicoe, J. E. (2009). Hydrokinetic energy conversion systems and assessment of horizontal and vertical axis turbines for river and tidal applications: A technology status review. *Applied Energy*, 86(10), 1823–1835. <https://doi.org/10.1016/j.apenergy.2009.02.017>
- Laws, N. D., & Epps, B. P. (2016). Hydrokinetic energy conversion: Technology, research, and outlook. *Renewable and Sustainable Energy Reviews*, 57, 1245–1259. <https://doi.org/10.1016/j.rser.2015.12.189>
- Li, Q., Maeda, T., Kamada, Y., Murata, J., Shimizu, K., Ogasawara, T., Nakai, A., & Kasuya, T. (2016). Effect of solidity on aerodynamic forces around straight-bladed vertical axis wind turbine by wind tunnel experiments (depending on number of blades). *Renewable Energy*, 96, 928–939. <https://doi.org/10.1016/j.renene.2016.05.054>
- Maître, T., Amet, E., & Pellone, C. (2013). Modeling of the flow in a Darrieus water turbine: Wall grid refinement analysis and comparison with experiments. *Renewable Energy*, 51, 497–512. <https://doi.org/10.1016/j.renene.2012.09.030>
- Malipeddi, A. R., & Chatterjee, D. (2012). Influence of duct geometry on the performance of Darrieus hydro-turbine. *Renewable Energy*, 43, 292–300. <https://doi.org/10.1016/j.renene.2011.12.008>

- McAdam, R. A., Houlsby, G. T., & Oldfield, M. L. G. (2013). Experimental measurements of the hydrodynamic performance and structural loading of the Transverse Horizontal Axis Water Turbine: Part 1. *Renewable Energy*, *59*, 105–114. <https://doi.org/10.1016/j.renene.2013.03.016>
- Mehling, H. (2017). *What is energy, and why is it conserved? A review, analysis, and suggested explanation and definition*. January, 18.
- Mosbahi, M., Ayadi, A., Chouaibi, Y., Driss, Z., & Tucciarelli, T. (2019). Performance study of a Helical Savonius hydrokinetic turbine with a new deflector system design. *Energy Conversion and Management*, *194*(April), 55–74. <https://doi.org/10.1016/j.enconman.2019.04.080>
- Munson, B. R., Young, D. F., & Okiishi, T. H. (1994). Fundamentals of fluid mechanics. *Fundamentals of Fluid Mechanics*. <https://doi.org/10.1201/b15874-2>
- Niebuhr, C. M., van Dijk, M., Neary, V. S., & Bhagwan, J. N. (2019). A review of hydrokinetic turbines and enhancement techniques for canal installations: Technology, applicability and potential. *Renewable and Sustainable Energy Reviews*, *113*(June), 109240. <https://doi.org/10.1016/j.rser.2019.06.047>
- Patel, V., Eldho, T. I., & Prabhu, S. V. (2019). Performance enhancement of a Darrieus hydrokinetic turbine with the blocking of a specific flow region for optimum use of hydropower. *Renewable Energy*, *135*, 1144–1156. <https://doi.org/10.1016/j.renene.2018.12.074>
- Phillips, T. S., & Roy, C. J. (2014). Richardson Extrapolation-Based Discretization Uncertainty Estimation for Computational Fluid Dynamics. *Journal of Fluids Engineering*, *136*(12), 121401. <https://doi.org/10.1115/1.4027353>
- Posa, A. (2020). Influence of Tip Speed Ratio on wake features of a Vertical Axis Wind Turbine. *Journal of Wind Engineering and Industrial Aerodynamics*, *197*(January), 104076. <https://doi.org/10.1016/j.jweia.2019.104076>
- Rezek, T. J., Camacho, R. G. R., Filho, N. M., & Limacher, E. J. (2021). Design of a Hydrokinetic Turbine Diffuser Based on Optimization and Computational Fluid Dynamics. *Applied Ocean Research*, *107*(August 2020), 102484. <https://doi.org/10.1016/j.apor.2020.102484>

- Roa, A. M., Aumelas, V., Maître, T., & Pellone, C. (2010). Numerical and experimental analysis of a darrieus-type cross flow water turbine in bare and shrouded configurations. *IOP Conference Series: Earth and Environmental Science*, 12, 012113. <https://doi.org/10.1088/1755-1315/12/1/012113>
- Saini, G., & Saini, R. P. (2020). Comparative investigations for performance and self-starting characteristics of hybrid and single Darrieus hydrokinetic turbine. *Energy Reports*, 6, 96–100. <https://doi.org/10.1016/j.egy.2019.11.047>
- Timilsina, A. B., Mulligan, S., & Bajracharya, T. R. (2018). Water vortex hydropower technology: a state-of-the-art review of developmental trends. *Clean Technologies and Environmental Policy*, 20(8), 1737–1760. <https://doi.org/10.1007/s10098-018-1589-0>
- Tunio, I. A., Shah, M. A., Hussain, T., Harijan, K., Mirjat, N. H., & Memon, A. H. (2020). Investigation of duct augmented system effect on the overall performance of straight blade Darrieus hydrokinetic turbine. *Renewable Energy*, 153, 143–154. <https://doi.org/10.1016/j.renene.2020.02.012>
- Wong, K. H., Chong, W. T., Poh, S. C., Shiah, Y. C., Sukiman, N. L., & Wang, C. T. (2018). 3D CFD simulation and parametric study of a flat plate deflector for vertical axis wind turbine. *Renewable Energy*, 129, 32–55. <https://doi.org/10.1016/j.renene.2018.05.085>